

Model-Aided INS With Sea Current Estimation for Robust Underwater Navigation

Øyvind Hegrenæs, *Member, IEEE*, and Oddvar Hallingstad, *Member, IEEE*

Abstract—This paper reports the development and experimental evaluation of a state-of-the-art model-aided inertial navigation system (MA-INS) for underwater vehicles. Together with real-time sea current estimation, the output from an experimentally validated kinetic vehicle model is integrated in the navigation system to provide velocity aiding for the INS. Additional aiding sources include ultrashort base line (USBL) acoustic positioning, pressure readings, and measurements from a Doppler velocity log (DVL) with bottom track. The performance of the MA-INS is evaluated on data from a field-deployed autonomous underwater vehicle (AUV). Several scenarios are examined, including removal or dropouts of USBL and DVL. The presented results verify that with merely an addition of software and no added instrumentation, it is possible to significantly improve the precision and robustness of an INS by utilizing the physical insight provided by a kinetic vehicle model. To the best of our knowledge, this paper reports the first experimental evaluation and practical application of a MA-INS for underwater vehicle navigation. The proposed approach improves underwater navigation capabilities both for systems lacking conventional velocity measurements, and for systems where the need for redundancy and integrity is important, e.g., during sensor dropouts or failures, or in case of emergency navigation. The MA-INS also represents a feasible step toward the solution to several prospective challenges in underwater navigation, including improved navigation in the midwater zone and increased level of autonomy and robustness.

Index Terms—Inertial navigation, Kalman filter, model aiding, sea current estimation, underwater vehicles, velocity aiding.

I. INTRODUCTION

WHILE remotely operated vehicles (ROVs) have been in operation for decades, autonomous underwater vehicles (AUVs) are today becoming accepted by an increasing number of users in both military and civilian institutions. Next to improved payload quality, much of this success is due to recent advances in navigation sensor technologies and fusion algorithms, which have enabled a significant progress in underwater navigation capabilities. An extensive review can be found in [1]. As stated in the same reference, the ABE underwater vehicle

Manuscript received January 31, 2009; revised February 21, 2010; accepted December 13, 2010. Date of current version May 27, 2011. This work was supported by the Research Council of Norway, Kongsberg Maritime, and Kongsberg Defence & Aerospace.

Associate Editor: D. J. Stilwell.

Ø. Hegrenæs is with Kongsberg Maritime Subsea, AUV Department, NO-3191 Horten, Norway (e-mail: oyvind.hegrenas@kongsberg.com).

O. Hallingstad is with the University Graduate Center at Kjeller, NO-2027 Kjeller, Norway (e-mail: oh@unik.no).

Color versions of one or more of the figures in this paper are available online at <http://ieeexplore.ieee.org>.

Digital Object Identifier 10.1109/JOE.2010.2100470

had at that time conducted 191 benthic surveys at midocean ridge sites at an average depth of 2000 m and with a navigation accuracy on the order of a few meters. A similar accuracy is achieved with the HUGIN AUVs, which by 2008 had accumulated a track record of around 200 000 km for the geophysical survey industry [2]. In addition, several other vehicles have also successfully been deployed. Despite these achievements, precise navigation remains a substantial challenge to all underwater platforms. The actual autonomy of many vehicles in existence today is also limited.

Kinsey *et al.* [1] state the following forthcoming challenges in underwater vehicle navigation: 1) multivehicle navigation; 2) improved near-bottom navigation; 3) further advances in state estimation research, in particular on model-based methodologies; 4) optimal survey and environmental estimation; and 5) improved navigation in the midwater zone, where acoustic time of flight systems and inertial measurement units (IMUs) have been the main tools for horizontal positioning to date. Besides these subjects, future research should also accommodate: 6) increased level of autonomy [3], including the use of terrain-based localization techniques and complementary velocity measurements for increased navigation accuracy and precision, robustness, and sustainability; and 7) development of methodologies for sensor and navigation system fault detection and isolation. Note that a complete distinction between the different challenges is difficult as they share many of the same subproblems. Advances in all of them will enable new applications of underwater vehicles, which earlier have been considered impractical or infeasible.

This paper presents an approach for aiding the inertial navigation system (INS) of an underwater vehicle using velocity measurements provided by an experimentally validated kinetic vehicle model. As illustrated in this work, the integration of the model velocities in the navigation system is an effective and inexpensive approach toward the solution to several of the aforementioned challenges, in particular 2)–6). Additional aiding is provided by an ultrashort base line (USBL) acoustic positioning system, ambient pressure readings, and velocity measurements from a Doppler velocity log (DVL) with bottom track. Global vehicle position measurements are obtained by combining differential global positioning system (DGPS) and USBL. In many practical cases, the position measurements will be unavailable for extended periods of time, and the INS then chiefly depends on external velocity aiding. Similarly, even when including a DVL, situations may arise where it fails to work or measurements are discarded due to decreased quality. This will, for instance, occur when operating in the midwater zone or over very rough bathymetry due to loss of bottom track. An illustrative

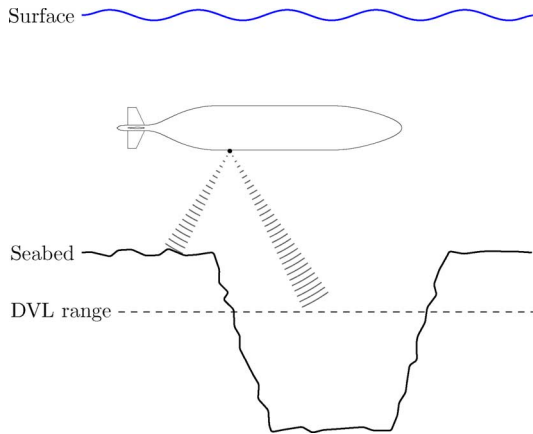


Fig. 1. Illustration of an AUV temporarily operating above the DVL sensor range, in this case caused by a distinct change in the bathymetry. The result is loss of bottom track and hence the feasibility of proper DVL-INS. This is also the outcome when operating in the midwater zone. The consequence of temporary loss of measurements from the DVL is investigated in Section IV-B4. The size of the AUV and the beams in the figure are not to scale.

example is given in Fig. 1. The inclusion of a kinetic vehicle model in the navigation system is found to be of great significance in all the aforementioned scenarios.

The performance of the integrated navigation system, which is applicable to a large group of submersibles, is evaluated on raw sensor data collected by the HUGIN 4500 AUV. The navigation system Kalman filter (KF) estimates the output errors of the INS as well as colored errors in the external aiding sources, including the kinetic vehicle model. Sea current estimation is also embedded in the navigation system. The experimental results verify that the accuracy, precision, and robustness of an INS are significantly improved by utilizing the physical insight provided by a kinetic vehicle model.

The possibility of using a kinetic vehicle model as an aiding tool is motivated by the initial feasibility study given in [4]. To the best of our knowledge, no results have been reported in the open literature on the experimental evaluation of a complete model-aided inertial navigation system (MA-INS), nor has its practical application to underwater navigation. This paper is a continuation to the work presented in [5]–[7], giving an extended and self-contained discussion and evaluation, and also elaborating on the development and validation of the kinetic vehicle model. The presented navigation system also incorporates a DVL with bottom track, along with the kinetic vehicle model, and it accommodates real-time sea current estimation and dynamic adaptation to degradation or improvement of all the INS aiding devices. In general, the integration of complementary velocity measurements enhances the precision, but most importantly, the robustness and sustainability of the navigation system.

For the remainder, MA-INS is used for short when discussing the MA-INS without distinguishing on additional aiding sensor. Similarly, the MA-INS with USBL and pressure sensor is denoted as USBL-MA-INS, and USBL-DVL-MA-INS when also including the DVL. We consider both configurations in this work, as well as USBL-DVL-INS and USBL-INS. This paper is furthermore organized as follows. Section I-A reviews work

on state estimation in underwater navigation and previously reported research on MA-INS. The kinetic vehicle model utilized for aiding the INS is presented in Section II. The same section describes the notation and kinematic relationships applied in the model and navigation system, along with important and often mistaken aspects related to sea current. The integrated INS with model aiding and DVL is presented in Section III. The experimental setup is described in Section IV, together with a comparative experimental evaluation of the proposed navigation system, where in particular, the performance of the navigation system with and without model aiding included is discussed.

A. Review on State Estimation and Model-Aided Navigation

In state estimation theory it is common to distinguish between stochastic and deterministic methodologies, where the former may be divided into Fisher and Bayesian approaches [8]. In the Fisher approach, the unknown quantity is viewed as a parameter for which no prior is available, and the value is estimated based solely on measurements having known statistics. The most common Fisher estimate is the maximum-likelihood (ML) method. An offline ML approach for estimating the horizontal position of a field-deployed AUV is reported in [9]. As for Bayesian estimation, it differs from the Fisher approach in that the estimated quantity or state is considered a random variable with a known prior distribution. As measurements are taken, the knowledge of the prior is fused with the known statistics of the measurement errors. This is done to obtain an estimate of the posterior distribution, and consequently of the respective state.

Unfortunately, an analytical solution to the Bayesian estimation problem is rarely obtainable for practical applications. Approximate methods are therefore usually needed. The most common example is the extended Kalman filter (EKF), which through a linearization yields a local approximation. See [10]–[12] for examples of EKF in underwater vehicle navigation. Alternative filtering techniques avoiding the potentially erroneous linearization include the point mass filter (PMF), the particle filter (PF), and the sigma-point Kalman filter (SPKF). The PMF uses a grid approach for approximating the posterior, while the PF and the SPKF rely upon a stochastic and deterministic sampling strategy, respectively. The posterior is estimated using a set of particles, sampled from known underlying distributions. An experimental evaluation of the PMF and the PF, applied to underwater terrain navigation, is given in [13], and similarly for the PF and the SPKF in [14]. Another comparison is reported through simulations in [15], where the EKF and the SPKF are integrated with the INS of an AUV. A further analysis of different state estimators is beyond the scope of this paper. The EKF was chosen in this work due to its flexibility and modest computational burden. For the nonlinearities considered herein the EKF is believed to be adequate. Through countless hours of operation with the HUGIN AUVs during the last decade, there are no indications to the contrary. The INS states are also reset occasionally to ensure small errors—a standard step for aided INS [8].

The application of state estimators to underwater navigation has primarily focused on employing purely kinematic plant models, i.e., models describing the vehicle motion without

considering the forces and moments causing it [12], [16], [17]. In the latter reference, a diffusion-based deterministic observer is proposed, which estimates the entire trajectory of the state as opposed to the state at a given instance. State estimators incorporating information from kinetic underwater vehicle models are rare. Model-based nonlinear deterministic observers utilizing knowledge of the vehicle dynamics together with disparate measurements are experimentally evaluated in [18], [19]. A related simulation study and comparison of two linear observers are reported in [20]. Another study is given on a conceptual level in [21], where a kinetic vehicle model of a ROV is included in the navigation system sensor fusion.

As for work on MA-INS, where the output from a kinetic vehicle model is used to aid the INS, the literature is scarce. Some reports are found related to aerial vehicles, where the navigation performance is evaluated in simulations [4], [22], [23]. What appears to be the first experimental evaluation of a complete MA-INS, and its practical application to underwater vehicle navigation, is reported in [5]–[7]. The application of model aiding in underwater navigation is also discussed in [24]. Morgado *et al.* present an analytical approach and evaluate the performance on simulated data. The effect of sea current is not taken into account in the latter reference.

For a further review on underwater vehicle navigation, including work on feature-based techniques and simultaneous localization and mapping (SLAM), the reader may refer to [1]. Additional discussions on sensor fusion techniques for underwater vehicle navigation are presented in [10] and [25].

II. UNDERWATER VEHICLE MODELING

Modeling of underwater vehicles is fairly complicated, and even when considered as a rigid body, an exact analysis is only possible by including the underlying infinite-dimensional dynamics of the surrounding fluid. While this can be done using partial differential equations, it still involves a formidable computational burden, infeasible for most practical applications. As a result, the conventional approach has been to use various finite-dimensional approximations, usually involving parameterized ordinary differential equations (ODEs). A brief review and historical recap is given in [26]. The same reference reports the experimental comparison of different models for a streamlined AUV. A frequently cited representation describing the six-degrees-of-freedom (6-DOF) motion of submarines is given in [27] and [28]. Other examples include [29] and [30]. In [31] and [32], models for isolated single degree of freedom motion are derived and validated. The amount of literature is extensive, and many other examples are readily available. It should also be mentioned that much of the work on modeling of surface vessels also applies to underwater vehicles. The same goes for low-speed aerodynamics since the Reynolds number for a typical underwater vehicle is comparable with that of an airplane in the lower subsonic range [33].

This section reports the analytical development and experimental validation of a 3-DOF kinetic model for a typical streamlined AUV. The notation and kinematic relationships applied in this paper are also presented. In Section III and IV, the model is used as a velocity aiding tool for the vehicle INS. The following is based partly on the results in [26] and [34].

A. Notation

A reference frame is denoted by $\{a\}$, where a is the frame in discussion. The coordinate-free position vector from the origin of $\{a\}$ to the origin of $\{b\}$ is given as \vec{p}_{ab} . Similarly, the coordinate-free angular velocity vector of $\{b\}$ relative to $\{a\}$ is written as $\vec{\omega}_{ab}$. For the linear velocity vector, the notation \vec{v}_{ab} is slightly ambiguous as it does not indicate how \vec{v}_{ab} is derived from \vec{p}_{ab} . As seen from (1), where the leading superscript denotes the frame where the differentiation is carried out, the choice of reference is in general not arbitrary

$$\frac{^a d}{dt} \vec{p}_{ab} = \frac{^b d}{dt} \vec{p}_{ab} + \vec{\omega}_{ab} \times \vec{p}_{ab}. \quad (1)$$

In light of this obscurity, the coordinate-free velocity vector of $\{b\}$ relative to $\{a\}$ may be written as $\vec{v}_{\underline{ab}}$ or $\vec{v}_{\underline{ab}}$, where the underline indicates the reference of differentiation. This is in agreement with the notation for kinematics proposed in [35].

A coordinate vector is a vector that can be described by its components in the Euclidian space \mathbb{R}^n . A coordinate vector is written in boldface. The position vector from $\{a\}$ to $\{b\}$ is then given as \mathbf{p}_{ab}^a , where the added superscript states in which frame the vector is decomposed. An example of linear and angular velocity vectors in coordinate form is \mathbf{v}_{ab}^b and $\boldsymbol{\omega}_{ab}^b$. Note that the time derivative of a coordinate vector does not require any additional notation since the differentiation is done in the immediate reference frame. If a prior reference of differentiation needs to be specified, this is done using the underline notation. This is illustrated in (2), where $[\vec{v}]^b \equiv \mathbf{v}^b$

$$\dot{\mathbf{v}}_{\underline{ab}}^b = \frac{d}{dt} \mathbf{v}_{\underline{ab}}^b = \frac{d}{dt} [\vec{v}_{\underline{ab}}]^b = \frac{d}{dt} \left[\frac{^a d}{dt} \vec{p}_{ab} \right]^b. \quad (2)$$

Recall that for any vectors $\mathbf{k}^a, \mathbf{k}^b \in \mathbb{R}^3$, $\mathbf{k}^b = \mathbf{R}_a^b \mathbf{k}^a$, where \mathbf{R}_a^b is the rotation matrix from $\{b\}$ to $\{a\}$, or alternatively, the coordinate transformation matrix from $\{a\}$ to $\{b\}$. A matrix \mathbf{R} is a valid rotation matrix if $\mathbf{R} \in SO(3)$, where

$$SO(3) = \left\{ \mathbf{R} \in \mathbb{R}^{3 \times 3} : \det(\mathbf{R}) = 1, \mathbf{R}^\top \mathbf{R} = \mathbf{R} \mathbf{R}^\top = \mathbf{I} \right\}. \quad (3)$$

All matrices, including the identity matrix \mathbf{I} , are written in bold caps. Another commonly applied set is defined as

$$so(3) = \{ \mathbf{S} \in \mathbb{R}^{3 \times 3} : \mathbf{S} = -\mathbf{S}^\top \}. \quad (4)$$

From (4), and for any vector $\mathbf{k} = [k_1, k_2, k_3]^\top$, the skew-symmetric matrix operator $\mathbf{S}(\cdot) : \mathbb{R}^3 \mapsto so(3)$ is given as

$$\mathbf{S}(\mathbf{k}) = \begin{bmatrix} 0 & -k_3 & k_2 \\ k_3 & 0 & -k_1 \\ -k_2 & k_1 & 0 \end{bmatrix}. \quad (5)$$

Note that for all $\mathbf{k}, \mathbf{j} \in \mathbb{R}^3$, it follows that $\mathbf{S}(\mathbf{k})\mathbf{j} \equiv \mathbf{k} \times \mathbf{j}$.

B. Kinematics

Let $\{m\}$ denote a local coordinate frame where the origin is fixed at the surface of the WGS-84 Earth ellipsoid, and the orientation is north–east–down (NED). Similarly, let $\{w\}$ denote a reference frame where the origin is fixed to, and translates with the water (due to sea current). The current is assumed irrotational throughout this paper, which implies that each infinitesimal

imal fluid element has zero angular velocity (spin). The frame $\{w\}$ is consequently defined such that it does not rotate relative to $\{m\}$. The sea current in this work is described entirely by the translational motion of $\{w\}$ relative to $\{m\}$. Recall that it is possible for a fluid traveling along a straight line to have vorticity, and similarly, for a fluid moving in a circle (or which changes direction) to be irrotational. For navigation purposes and INS, two additional reference frames are often used. The Earth-centered–Earth-fixed (ECEF) frame is denoted $\{e\}$. The second frame $\{l\}$ is a wander azimuth frame. It is similar to $\{m\}$, but its origin is always located directly above the vehicle at the surface of the Earth ellipsoid. It is furthermore defined such that it has zero angular velocity relative to the rotating Earth about its z -axis. A last frame $\{b\}$ is a body-fixed frame where the axes coincide with the principal axes of the vehicle, and the origin is located at the vehicle center of buoyancy (CB). Finally, note that a vehicle will not rotate as it translates in an irrotational fluid, hence the irrotational current assumption implies that $\vec{\omega}_{mb} = \vec{\omega}_{wb}$.

Based on the notation and reference coordinate frames described above, a general expression of the vehicle position may be written in coordinate-free form as

$$\vec{p}_{mb} = \vec{p}_{mw} + \vec{p}_{wb}. \quad (6)$$

By incorporating (1), the time derivative of (6) is found to be

$$\frac{^m d}{dt} \vec{p}_{mb} = \frac{^m d}{dt} \vec{p}_{mw} + \frac{^w d}{dt} \vec{p}_{wb} + \vec{\omega}_{mw} \times \vec{p}_{wb} \quad (7)$$

where $\vec{\omega}_{mw}$ equals zero due to the assumption of irrotational current. In coordinate form, this is equivalent to \mathbf{R}_w^m being time invariant. Written in terms of velocities, (7) yields

$$\vec{v}_{mb} = \vec{v}_{mw} + \vec{v}_{wb} \quad (8)$$

which decomposed in $\{b\}$ gives the velocity relationship

$$\vec{v}_{mb}^b = \mathbf{R}_m^b \vec{v}_{mw}^m + \vec{v}_{wb}^b. \quad (9)$$

Following along the same lines as above, a second important velocity relationship is given as

$$\vec{v}_{eb}^l = \vec{v}_{ew}^l + \mathbf{R}_b^l \vec{v}_{wb}^b. \quad (10)$$

Note that \vec{v}_{mb}^b equals \vec{v}_{eb}^l since $\{m\}$ is fixed relative to $\{e\}$.

The correspondence between the variables above and the nomenclature established by the Society of Naval Architects and Marine Engineers (SNAME) [36] is given in Table I, and an illustrative example of different speed entities along the x -axis of $\{b\}$ is shown in Fig. 2.

Property 1: For a slowly varying current of small magnitude, or for vehicles moving at a fixed orientation or attitude, it is found that $\dot{\vec{v}}_{mb}^b$ and $\dot{\vec{v}}_{wb}^b$ are approximately equal.

Proof: Taking the derivative of both sides of (9) yields

$$\dot{\vec{v}}_{mb}^b = \mathbf{R}_m^b \dot{\vec{v}}_{mw}^m + \dot{\mathbf{R}}_m^b \vec{v}_{mw}^m + \dot{\vec{v}}_{wb}^b. \quad (11)$$

TABLE I
NOMENCLATURE

Description	Variable	Entries*
Local NED vehicle position	\vec{p}_{mb}^m	(x, y, z)
Arm from $\{b\}$ to vehicle CG	\vec{p}_{bg}^b	(x_g, y_g, z_g)
Vehicle attitude (roll, pitch, yaw)	Θ	(ϕ, θ, ψ)
Vehicle angular velocity	$\vec{\omega}_{mb}^b = \vec{\omega}_{eb}^b = \vec{\omega}_{wb}^b$	(p, q, r)
Earth-relative linear velocity	$\vec{v}_{mb}^b = \vec{v}_{eb}^b$	(u, v, w)
Earth-relative linear velocity	$\vec{v}_{mb}^l = \vec{v}_{eb}^l$	(u^l, v^l, w^l)
Water-relative linear velocity	\vec{v}_{wb}^b	(u_r, v_r, w_r)
Current velocity	$\vec{v}_{mw}^b = \vec{v}_{ew}^b$	(u_c, v_c, w_c)
Current velocity	$\vec{v}_{mw}^l = \vec{v}_{ew}^l$	(u_c^l, v_c^l, w_c^l)
External forces on vehicle	\mathbf{f}^b	(X, Y, Z)
External moments on vehicle	\mathbf{m}^b	(K, M, N)

* Based on SNAME [36] notation

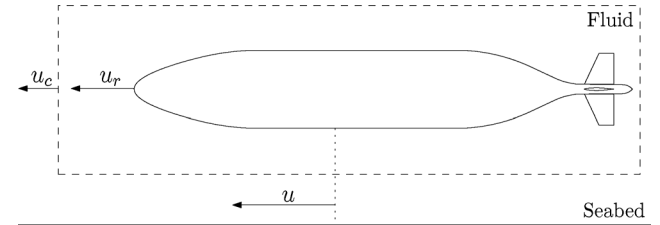


Fig. 2. Speed entities along x -axis of $\{b\}$: Water-relative speed u_r , current speed u_c , and ground speed u . HUGIN 4500 AUV profile used for illustration.

From the rule of time differentiation of rotation matrices [37], and under the assumption of a slowly varying current, i.e., $\dot{\vec{v}}_{mw}^m \approx 0$, (11) may be rewritten as

$$\begin{aligned} \dot{\vec{v}}_{mb}^b &\approx \dot{\vec{v}}_{wb}^b + \dot{\mathbf{R}}_m^b \vec{v}_{mw}^m \\ &= \dot{\vec{v}}_{wb}^b + \mathbf{S}(\vec{\omega}_{bm}^b) \mathbf{R}_m^b \vec{v}_{mw}^m \\ &= \dot{\vec{v}}_{wb}^b - \mathbf{S}(\vec{\omega}_{mb}^b) \mathbf{R}_m^b \vec{v}_{mw}^m. \end{aligned} \quad (12)$$

It follows that $\dot{\vec{v}}_{mb}^b \approx \dot{\vec{v}}_{wb}^b$ if either $\vec{\omega}_{mb}^b$ or \vec{v}_{mw}^m is sufficiently small. For level flights in the geographical horizontal plane, i.e., for steady low-pitch–low-roll flights, the condition on the angular velocity is equivalent to low yaw rates. \square

C. Vehicle Maneuvering Model

The HUGIN 4500 AUV is used as a case study in this work. The profile of the vehicle is outlined in Fig. 2. The bare hull is a body of revolution, and the cruciform tail fin configuration is top–bottom, portstarboard symmetric. Additional information and vehicle particulars are given in Section IV-A. We consider a 3-DOF kinetic model for describing the vehicle motion in surge, sway, and yaw. We assume negligible coupling from velocity in heave, and angular rates in roll and pitch, which are reasonable assumptions for normal operations with the HUGIN 4500 AUV. Additional DOF should be included for strongly coupled and coordinated maneuvers. When deriving the model, we apply the additional assumptions that: 1) the vehicle can be modeled as a rigid body of constant mass; 2) the Earth rotation is omitted (it is included in the INS), hence $\{e\}$ and $\{m\}$ are considered inertial; 3) the vehicle is deeply submerged in unbounded fluid,

hence we neglect boundary effects; 4) the fluid is uniform and incompressible; 5) the pressure gradient in the accelerating fluid is disregarded when considering the vehicle added mass; 6) the vehicle is subject to an environmental disturbance in the form of irrotational current; and 7) no parts of the actuation do saturate or stall.

A generic representation of the equations of motion (EOM) for a rigid body may be written as [38]

$$\mathbf{M}_{RB}\dot{\boldsymbol{\nu}} + \mathbf{C}_{RB}(\boldsymbol{\nu})\boldsymbol{\nu} = \boldsymbol{\tau}_{RB} \quad (13)$$

where \mathbf{M}_{RB} is the rigid body system inertia matrix and \mathbf{C}_{RB} is the corresponding matrix of Coriolis-centripetal terms. Complete expressions and various properties of the matrices are found in the latter reference. In the 6-DOF case, and based on the nomenclature in Table I, the generalized vectors of external forces and moments, and Earth-relative velocities, are given as $\boldsymbol{\tau}_{RB} = [X, Y, Z, K, M, N]^\top$ and $\boldsymbol{\nu} = [u, v, w, p, q, r]^\top$, respectively. Similarly, a generalized vector of water-relative velocities is defined as $\boldsymbol{\nu}_r = [u_r, v_r, w_r, p, q, r]^\top$, where it is seen that only the linear or translational parts of $\boldsymbol{\nu}$ and $\boldsymbol{\nu}_r$ differ. This is due to the assumption of an irrotational current.

Property 2: In the case of a constant irrotational current, using $\boldsymbol{\nu}$ or $\boldsymbol{\nu}_r$ in (13) is equivalent in the sense that

$$\mathbf{M}_{RB}\dot{\boldsymbol{\nu}} + \mathbf{C}_{RB}(\boldsymbol{\nu})\boldsymbol{\nu} = \mathbf{M}_{RB}\dot{\boldsymbol{\nu}}_r + \mathbf{C}_{RB}(\boldsymbol{\nu}_r)\boldsymbol{\nu}_r. \quad (14)$$

Proof: Following along the same lines as in (11) and (12), and under the assumption of a constant current, i.e., $\dot{\boldsymbol{\nu}}_{mb}^m = \mathbf{0}$, it is straightforward to derive the relationship

$$\begin{aligned} \dot{\boldsymbol{\nu}}_{mb}^b &= \dot{\boldsymbol{\nu}}_{wb}^b + \dot{\mathbf{R}}_m^b \boldsymbol{\nu}_{mb}^m \\ &= \dot{\boldsymbol{\nu}}_{wb}^b - \mathbf{S}(\boldsymbol{\omega}_{mb}^b) \boldsymbol{\nu}_{mb}^b. \end{aligned} \quad (15)$$

From (9), (15), and the nomenclature in Table I, it follows that

$$\dot{\boldsymbol{\nu}} = \begin{bmatrix} \dot{u}_r + rv_c - qw_c \\ \dot{v}_r + pw_c - ru_c \\ \dot{w}_r + qu_c - pv_c \\ \dot{p} \\ \dot{q} \\ \dot{r} \end{bmatrix}, \quad \boldsymbol{\nu} = \begin{bmatrix} u_r + u_c \\ v_r + v_c \\ w_r + w_c \\ p \\ q \\ r \end{bmatrix}. \quad (16)$$

The desired result is obtained by direct substitution for $\dot{\boldsymbol{\nu}}$ and $\boldsymbol{\nu}$ in (14), i.e., using (16) and after canceling terms. Note that the result is valid for the general rigid body EOM in (13). \square

For the 3-DOF model, the generalized force and velocity vectors simplify to $\boldsymbol{\tau}_{RB} = [X, Y, N]^\top$, $\boldsymbol{\nu} = [u, v, r]^\top$, and $\boldsymbol{\nu}_r = [u_r, v_r, r]^\top$. The vector from the origin $\{b\}$ to the vehicle center of gravity (CG) is given as $\mathbf{p}_{bg}^b = [0, 0, z_g]^\top$, hence

$$\mathbf{M}_{RB} = \begin{bmatrix} m & 0 & 0 \\ 0 & m & 0 \\ 0 & 0 & I_z \end{bmatrix} \quad (17)$$

$$\mathbf{C}_{RB} = \begin{bmatrix} 0 & 0 & -mv \\ 0 & 0 & mu \\ mv & -mu & 0 \end{bmatrix} \quad (18)$$

where m is the mass of the vehicle in water and I_z is the vehicle moment of inertia about the z -axis of $\{b\}$. The difficulty in modeling a submersible arises when expressing the right-hand side of (13). One possibility is to decompose $\boldsymbol{\tau}_{RB}$ into forces and moments produced by the propulsion system and the control surfaces, and hydrodynamic forces and moments resulting from the reaction between the fluid and the vehicle. It is in the evaluation of the hydrodynamics that the greatest source of uncertainty lies, due to the fact that one is adopting a finite-dimensional approximation to the underlying infinite-dimensional dynamics of the fluid.

A 3-DOF maneuvering model for the HUGIN 4500 (and other streamlined underwater vehicles) can be written as

$$\mathbf{M}_{RB}\dot{\boldsymbol{\nu}} + \mathbf{C}_{RB}(\boldsymbol{\nu})\boldsymbol{\nu} = \boldsymbol{\tau} - \mathbf{M}_A\dot{\boldsymbol{\nu}}_r - \mathbf{C}_A(\boldsymbol{\nu}_r)\boldsymbol{\nu}_r - \mathbf{d}(\boldsymbol{\nu}_r) - \mathbf{g}(\Theta) + \mathbf{b} \quad (19)$$

where the right-hand side accounts for external forces and moments from actuation, added mass, linear and nonlinear hydrodynamic damping (lift and drag), weight and buoyancy, and time-invariant force and moment biases. Note that the external forces and moments depend on the relative motion between the vehicle and the water, opposed to the left-hand side of (19), which depends on the inertial vehicle motion. The terms in (19) and some of their properties are as follows.

1) The contribution from the control surfaces is given as

$$\boldsymbol{\tau}_C = \begin{bmatrix} X_{\delta\theta uu} (\delta r_t^2 + \delta r_b^2 + \delta e_p^2 + \delta e_s^2) u_r^2 \\ Y_{\delta\theta uu} (\delta r_t + \delta r_b) u_r^2 + Y_{ur\delta} u_r v_r + Y_{uv\delta} u_r v_r \\ N_{\delta\theta uu} (\delta r_t + \delta r_b) u_r^2 + N_{ur\delta} u_r v_r + N_{uv\delta} u_r v_r \end{bmatrix} \quad (20)$$

where the deflections of the top and bottom rudders and port and starboard elevators are given as δr_t , δr_b , δe_p , and δe_s , respectively. The forces and moments produced by the single aft mounted propeller are given as

$$\boldsymbol{\tau}_P = \begin{bmatrix} X_{|n|n} n |n| n + X_{|n|u} n |(1-w)u_r| \\ 0 \\ 0 \end{bmatrix} \quad (21)$$

where the propeller rotation rate is denoted by n and w is the wake fraction number. The total control forces and moments are calculated as $\boldsymbol{\tau} = \boldsymbol{\tau}_C + \boldsymbol{\tau}_P$.

2) The system inertia matrix of added mass is denoted \mathbf{M}_A , and \mathbf{C}_A is the corresponding hydrodynamic Coriolis and centripetal matrix. The matrices are given as

$$\mathbf{M}_A = \begin{bmatrix} -X_{\dot{u}} & 0 & 0 \\ 0 & -Y_{\dot{v}} & -Y_{\dot{r}} \\ 0 & -N_{\dot{v}} & -N_{\dot{r}} \end{bmatrix} \quad (22)$$

$$\mathbf{C}_A = \begin{bmatrix} 0 & 0 & Y_{\dot{r}} r + Y_{\dot{v}} v_r \\ 0 & 0 & -X_{\dot{u}} u_r \\ -Y_{\dot{r}} r - Y_{\dot{v}} v_r & X_{\dot{u}} u_r & 0 \end{bmatrix}. \quad (23)$$

3) The damping terms are among the most complex ones to model. The lift and drag forces and moments on the hull arising from circulatory effects (at low angles of incidence, prior to flow separation) are described as

$$\mathbf{d}_l = \begin{bmatrix} -X_{vr} v_r r - X_{vv} v_r^2 - X_{rr} r^2 \\ -Y_{uv} u_r v_r - Y_{ur} u_r r \\ -N_{uv} u_r v_r - N_{ur} u_r r \end{bmatrix}. \quad (24)$$

Interference effects from the fins on the hull are not explicitly accounted for. Linear skin friction terms, which dominate at low speed, are represented as

$$\mathbf{D}_L = \begin{bmatrix} -X_u & 0 & 0 \\ 0 & -Y_v & -Y_r \\ 0 & -N_v & -N_r \end{bmatrix}. \quad (25)$$

Similarly, turbulent or nonlinear skin friction, and damping due to vortex shedding (cross-flow drag and nonlinear lift from fluid separation), are included in

$$\mathbf{D}_{NL} = \begin{bmatrix} -X_{|u|u}|u_r| & 0 & 0 \\ 0 & -Y_{|v|v}|v_r| & -Y_{|r|r}|r| \\ 0 & -N_{|v|v}|v_r| & -N_{|r|r}|r| \end{bmatrix}. \quad (26)$$

The axial components of \mathbf{D}_L and \mathbf{D}_{NL} account for friction from the hull and the fins. The total hydrodynamic damping is finally found as $\mathbf{d} \triangleq \mathbf{d}_l + (\mathbf{D}_L + \mathbf{D}_{NL})\boldsymbol{\nu}_r$.

- 4) Restoring forces and moments are represented as

$$\mathbf{g} = \begin{bmatrix} (W - B) \sin(\theta) \\ -(W - B) \cos(\theta) \sin(\phi) \\ 0 \end{bmatrix} \quad (27)$$

where W and B denote vehicle weight and buoyancy.

- 5) Constant biases due to unmodeled effects are given as

$$\mathbf{b} = \begin{bmatrix} X_b \\ Y_b \\ N_b \end{bmatrix}. \quad (28)$$

For (19), one must decide upon using either the relative velocity $\boldsymbol{\nu}_r$ or the inertial velocity $\boldsymbol{\nu}$ as the state. If the assumptions in Property 1 hold, (19) may be restated as

$$\mathbf{M}\dot{\boldsymbol{\nu}}_r = \boldsymbol{\tau} - \mathbf{c}(\boldsymbol{\nu}, \boldsymbol{\nu}_r) - \mathbf{d}(\boldsymbol{\nu}_r) - \mathbf{g}(\Theta) + \mathbf{b} \quad (29)$$

where for simplicity $\mathbf{M} \triangleq \mathbf{M}_{RB} + \mathbf{M}_A$ and

$$\mathbf{c}(\boldsymbol{\nu}, \boldsymbol{\nu}_r) \triangleq \mathbf{C}_{RB}(\boldsymbol{\nu})\boldsymbol{\nu} + \mathbf{C}_A(\boldsymbol{\nu}_r)\boldsymbol{\nu}_r. \quad (30)$$

Since the term $\mathbf{c}(\boldsymbol{\nu}, \boldsymbol{\nu}_r)$ is a function of both $\boldsymbol{\nu}_r$ and $\boldsymbol{\nu}$, the current must be measured or estimated. Recall that $\boldsymbol{\nu}$ can be found from (9), once the current, vehicle attitude, and $\boldsymbol{\nu}_r$ are known. In the aided INS studied in this paper, the KF accommodates real-time current estimation. With the assumption of a constant irrotational current and negligible pitch and roll rates, it is easily verified that Property 2 also applies to (19), in which case the model further simplifies to

$$\mathbf{M}\dot{\boldsymbol{\nu}}_r = \boldsymbol{\tau} - \mathbf{c}(\boldsymbol{\nu}_r) - \mathbf{d}(\boldsymbol{\nu}_r) - \mathbf{g}(\Theta) + \mathbf{b}. \quad (31)$$

This is equal to (29), with $\boldsymbol{\nu}$ replaced by $\boldsymbol{\nu}_r$. The expression is also valid for the zero-current case, for which $\boldsymbol{\nu} = \boldsymbol{\nu}_r$.

The different 3-DOF models above are typical gray-box models where the vehicle motion is described by a set of parameterized ODEs. The mathematical structure of the models is presumed known, but several of the parameters are unknown and must be identified. Since the coefficients $X_{(\cdot)}, Y_{(\cdot)}, N_{(\cdot)}$ enter linearly, it is for parameter identification purposes possible to rewrite the models by means of a known observation

vector $\mathbf{y} \in \mathbb{R}^3$, a known linear regressor $\Phi \in \mathbb{R}^{3 \times p}$, and an unknown parameter vector $\boldsymbol{\varphi} \in \mathbb{R}^p$, that is

$$\mathbf{y}(t) = \Phi(t)\boldsymbol{\varphi}. \quad (32)$$

In Section II-D, the parameter vector with $p = 20$ is given as

$$\boldsymbol{\varphi} = [X_u, X_{|u|u}, X_{vr}, X_{vv}, X_{rr}, X_b, Y_v, Y_r, Y_{|v|v}, Y_{|r|r}, Y_{uv}, Y_{ur}, Y_b, N_v, N_r, N_{|v|v}, N_{|r|r}, N_{uv}, N_{ur}, N_b]^\top. \quad (33)$$

After determining all the unknown parameters, a standard numerical integration routine (see, e.g., [37]) can be used to recover the state. That is, model-based measurements of the water-relative velocity in surge and sway, as well as the yaw rate, can be attained from known control signals (fins and propulsion), vehicle roll and pitch, and current (when appropriate). Control or actuation signals, and vehicle roll and pitch are usually accurately measured.

D. Parameter Identification and Model Cross Validation

The kinetic vehicle models discussed above contain unknown coefficients for which values need to be estimated. For the parameter identification in this paper, data collected during several sea trials with the HUGIN 4500 were used. Details can be found in [26]. The current at the test site was found to be slowly varying and of a magnitude in the order of a few centimeters per second. The model structure in (29) was consequently found suitable for the parameter identification task. Note that the coefficients in (29) also apply to (31). The latter model was found adequate when applying the vehicle model as a navigation aiding tool for the INS in Section III-C.

Prior to fitting the model to the full-scale experimental data, it is necessary to obtain an estimate of the current, and thereafter, an estimate of the vehicle water-relative velocity. This has to be done since HUGIN 4500 currently does not measure the water-relative velocity directly. Since all the data were collected at sea, the Earth-relative and water-relative vehicle velocities usually differ. In [34], the current was successfully estimated by utilizing the measured attitude and Earth-relative linear velocity of the vehicle. Steady-state maneuvering characteristics for HUGIN 4500 were also obtained in the same reference, and later utilized in [26] as part of an alternative current estimation approach. Both approaches are used in the model development and validation herein. Once the current is known, the water-relative velocity can be found from (9). An example of experimental velocity data before and after current has been compensated for is shown in Fig. 3.

For the vehicle model in (29), the terms in (32) are given as

$$\mathbf{y}(t) = \mathbf{M}\dot{\boldsymbol{\nu}}_r + \mathbf{c}(\boldsymbol{\nu}, \boldsymbol{\nu}_r) + \mathbf{g}(\Theta) - \boldsymbol{\tau} \quad (34)$$

$$\Phi(t)\boldsymbol{\varphi} = \mathbf{b} - \mathbf{d}(\boldsymbol{\nu}_r) \quad (35)$$

where if we define $\mathbf{U}(t) \triangleq \mathbf{b} - \mathbf{d}(\boldsymbol{\nu}_r)$, it trivially follows that

$$\Phi_{ij}(t) = \frac{\partial \mathbf{U}_i(t)}{\partial \boldsymbol{\varphi}_j}, \quad \text{for } \begin{cases} i = 1, \dots, 3 \\ j = 1, \dots, 20. \end{cases} \quad (36)$$

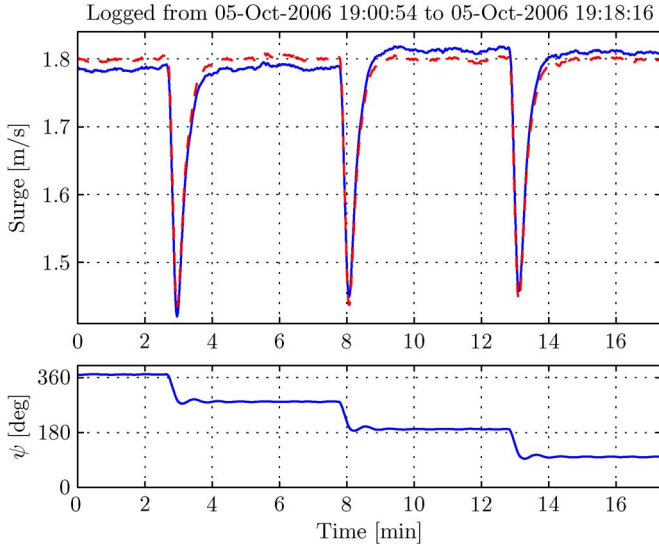


Fig. 3. Earth-relative surge velocity u (solid) and water-relative surge velocity u_r (dashed), both in the vehicle CB. The vehicle followed a square shaped trajectory, at a constant propeller RPM. The stationary value of u depends on the vehicle course, due to a nonzero current. In [34], the current speed and direction were found to be 0.02 m/s and 144.6°, 180° being south.

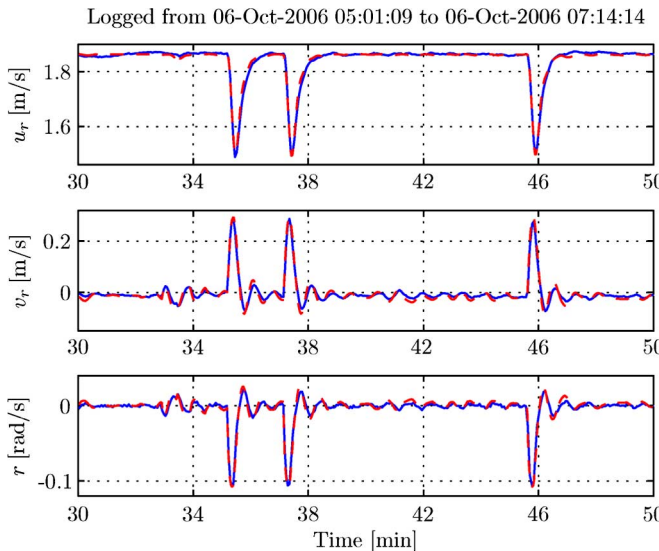


Fig. 4. Water-relative vehicle velocity in surge, sway, and yaw. All in the vehicle CB. The model outputs (dashed red) closely follow the experimental data (solid blue). The data correspond to the fourth 180° turn and subsequent 90° turn in Figs. 9 and 14. No parts of the cross-validation data were used in the model development and identification stage.

With exception of φ given in (33), all the terms in (32) are measured or assumed known. The added mass terms were calculated using the methodologies reported in [39]–[41]. Similarly, the contribution and coefficients for the control surfaces were approximated from semi-empirical relationships found in [42]–[45]. As for the propulsion system, the parameters were obtained experimentally [46].

In summary, the parameter identification task is to estimate the parameter vector φ in the continuous-time model structure (32), given observations of the vehicle acceleration, velocities

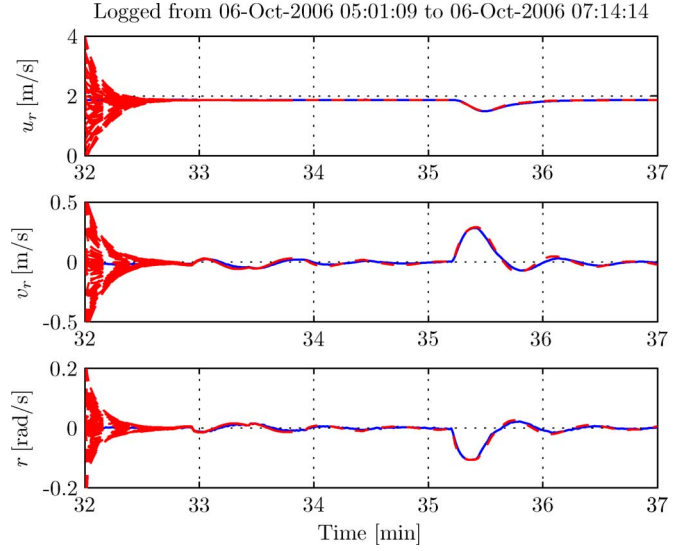


Fig. 5. Water-relative vehicle velocity in surge, sway, and yaw. Subset of the data shown in Fig. 4. The model outputs (dashed red) closely follow the experimental data (solid blue). As illustrated, the steady-state model outputs are insensitive to initial conditions (for all practical cases), hence the model may be initialized independently of the state of other external sensors.

and orientation, as well as actuator readings. Our identification approach is based on the least squares (LS) criterion

$$\hat{\varphi} = \arg \min_{\varphi} \sum_{k=1}^N [\mathbf{y}(t_k) - \Phi(t_k)\varphi]^T [\mathbf{y}(t_k) - \Phi(t_k)\varphi] \quad \text{subject to: } \underline{\varphi} \leq \varphi \leq \bar{\varphi} \quad (37)$$

where t_k denotes the time at sample k , and $\underline{\varphi}$ and $\bar{\varphi}$ are lower and upper bounds on the coefficient vector, respectively. Prior to applying (37), the appropriate measurements were outlier filtered and smoothed using the postprocessing tool NavLab [47]. This was done to enhance the accuracy. Additional information on NavLab is given in Section IV-A.

A standard step in parameter identification is to validate the model on independent data sets, not used during the identification stage. A cross-validation example is shown in Fig. 4. The identified model was found to accurately predict the vehicle motion. For further details on the data used for identifying the parameters, and for an extended treatment on the experimental cross validation, the reader is referred to [26].

When utilizing a kinetic vehicle model for simulation purposes or as an aiding tool for an INS, the sensitivity to initial conditions is also of interest. As can be seen in Fig. 5, the steady-state outputs from the model are identical for the different combinations of initial conditions. In a navigation setting, this means that the model may be initialized independently of the current state of the INS or other external sensors.

III. UNDERWATER VEHICLE INERTIAL NAVIGATION

IMUs, time-of-flight acoustics, velocity logs, and global positioning systems (GPSs) are all common means for precision underwater navigation. As pointed out by Kinsey *et al.* [1], none of

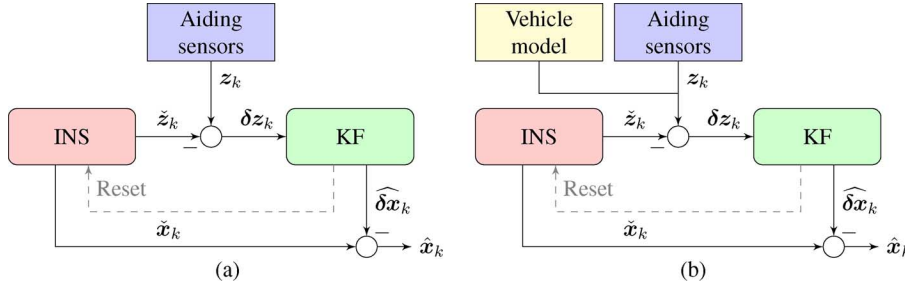


Fig. 6. High-level system outline. (a) Conventional aided INS. (b) MA-INS. The vehicle model is treated analogously to an external aiding sensor.

these techniques is perfect however, and a combination of them is usually employed in practice.

As an addition to the conventional underwater vehicle navigation techniques, this section reports the concept of a MA-INS. A second velocity aid is also integrated in the system using a DVL with bottom track. As is illustrated in Section IV-B, the application of complementary measurements enhances the precision, and even more importantly, the robustness and sustainability of the integrated navigation system. In systems without DVL, the use of model aiding significantly increases both the precision and feasible operating time span.

A. Principles of INS

An INS calculates position, velocity, and attitude using high-frequency data from an IMU, which typically consists of three accelerometers measuring specific force and three gyros measuring angular rate, all relative to the inertial space. Due to inherent errors in the gyros and accelerometers, the solution of the navigation equations embedded in the INS will have an unbounded drift unless counteracted. A performance measure for an INS is given by its pure inertial drift in position, where the divergence rate depends on the IMU quality. A navigation grade INS drifts in the order of one nautical mile per hour.

Since an INS is a diverging system, it requires an aiding framework to bound the growth of its errors. Standard components such as compass and pressure sensor are usually included, where the latter effectively bounds the vertical position drift. Navigation in the geographical horizontal plane is more challenging, and the main aiding methods to date involve time-of-flight acoustics, surface GPS, and DVL [1]. An overview of different INS aiding tools available for the HUGIN AUVs (and other submersibles) is given in [10]. Model aiding, as presented in this paper, is a new addition to this set of tools.

An outline of a conventional aided INS is shown in Fig. 6(a), where the KF input is taken as the difference between the output from the appropriate aiding sensors and the INS. A perturbation method is used in this work for deriving the error states of the INS navigation equations, where the errors are defined as the difference between the calculated and true position, orientation, and velocity of the vehicle. The states are included in the KF with the assumptions of small errors, i.e., first-order approximation. Besides modeling the INS errors, the KF also estimates the colored noise in the gyros, accelerometers, and the external aiding sensors. The sea current is also estimated in real time. The derivation of the KF measurement and process equations associated with the DVL, vehicle model, and the sea current are given

subsequently. The derivation of the measurement and process equations for the other aiding sensors follow analogously.

B. DVL Aiding

If within sensor range, the DVL measures the vehicle velocity relative to the seabed along four acoustic beams. The information obtained from the pings in each beam is combined to calculate the linear vehicle velocity. Bottom track from at least three beams is required.

The amount of literature on error sources and the use of DVL in underwater navigation is extensive. The reader is referred to [1] and references therein. Some additional references include [10] and [48]. Of underwater navigation systems incorporating DVL one may often distinguish between those based on INS, and those carrying out more traditional dead-reckoning by combining attitude information and DVL directly. Only the first case is considered in this work.

1) Measurement and Process Equations: The generalized vector of discrete inputs to the KF in Fig. 6 is given as

$$\delta z_k \triangleq z_k - \check{z}_k \quad (38)$$

where $(\check{\cdot})$ denotes a calculated variable, in this case from the INS. Note that the number of entries of z_k varies with the measurement availability at a particular sample instant k . For the linear velocity associated with the DVL, we then get

$$\delta z_{\text{vel}}^{\text{DVL}} \triangleq z_{\text{vel}}^{\text{DVL}} - \check{z}_{\text{vel}}^{\text{INS}} \quad (39)$$

where the sample index has been dropped for brevity. Substituting for the variables on the right-hand side of (39) yields

$$\delta z_{\text{vel}}^{\text{DVL}} = \check{R}_b^l \check{v}_{eb}^b - \check{v}_{eb}^l \quad (40)$$

where $(\check{\cdot})$ denotes a measured quantity. The variables \check{v}_{eb}^l and \check{R}_b^l stem from the INS, and \check{v}_{eb}^b is the Earth-relative velocity measured by the DVL. Note that any misalignment between the DVL instrument frame and the body frame, as well as scale effects due to erroneous speed of sound in the DVL, should be sought compensated for prior to applying \check{v}_{eb}^b in the KF.

A calculated or measured variable may be considered as a sum of its true value and a corresponding error, that is

$$(\check{\cdot}) = (\cdot) + \delta(\cdot) \quad \text{and} \quad (\tilde{\cdot}) = (\cdot) + \delta(\cdot). \quad (41)$$

Substituting with errors and true values in (40) yields

$$\delta z_{\text{vel}}^{\text{DVL}} = \delta R_b^l R_b^l \left(v_{eb}^b + \delta v_{eb}^b \right) - \left(v_{eb}^l + \delta v_{eb}^l \right) \quad (42)$$

where $\delta\mathbf{R}_b^l \in SO(3)$ is a measure of the deviation between the true rotation matrix and the rotation matrix calculated by the INS. For small errors, it can be shown that $\delta\mathbf{R}_b^l \approx \mathbf{I} + \mathbf{S}(\mathbf{e}_{lb}^l)$, where \mathbf{e}_{lb}^l is a vector of angle-axis errors [49]. Returning to (42), the final expression for the measurement equation associated with the DVL may be written to first order as

$$\delta\mathbf{z}_{vel}^{DVL} = \mathbf{R}_b^l \delta\mathbf{v}_{eb}^b - \delta\mathbf{v}_{eb}^l - \mathbf{S}(\mathbf{v}_{eb}^l) \mathbf{e}_{lb}^l. \quad (43)$$

Both $\delta\mathbf{v}_{eb}^l$ and \mathbf{e}_{lb}^l are included as states in the KF process equation. Note that (43) is not directly realizable since it depends on the true velocity and orientation, i.e., \mathbf{v}_{eb}^l and \mathbf{R}_b^l . When implementing the KF, the best *a priori* estimates are used in lieu, calculated according to

$$\bar{\mathbf{v}}_{eb}^l \triangleq \check{\mathbf{v}}_{eb}^l - \overline{\delta\mathbf{v}}_{eb}^l \quad \text{and} \quad \bar{\mathbf{R}}_b^l \triangleq [\mathbf{I} - \mathbf{S}(\bar{\mathbf{e}}_{lb}^l)] \check{\mathbf{R}}_b^l \quad (44)$$

where (\cdot) denotes the most recent or best *a priori* estimate prior to the KF measurement update or correction.

It is assumed in this work that the DVL output error $\delta\mathbf{v}_{eb}^b$ can be modeled as the sum of colored noise and zero-mean white noise. The entries of $\delta\mathbf{v}_{eb}^b$ are considered uncorrelated. If we let $\Delta\mathbf{v}_{(\cdot)}$ and $\xi_{(\cdot)}$ denote the colored and white noises, respectively, the error can be expressed as

$$\delta\mathbf{v}_{eb}^b = \Delta\mathbf{v}_{eb}^b + \xi_{v_{eb}^b}. \quad (45)$$

While white noise is isolated in time, a colored process is local in time since its value at one instant also depends on prior values. Numerous correlation models can be used, depending on the known or presumed noise characteristics [50], [51]. The colored noise in (45) is embedded in the KF as a zero-mean first-order Markov process driven by white noise, that is

$$\dot{\Delta\mathbf{v}}_{eb}^b = -\mathbf{T}_{\Delta\mathbf{v}_{eb}^b}^{-1} \Delta\mathbf{v}_{eb}^b + \gamma_{\Delta\mathbf{v}_{eb}^b}. \quad (46)$$

The success of the Markov model relies on the determination of the parameter $\mathbf{T}_{(\cdot)}$ and the white noise $\gamma_{(\cdot)}$. The matrix $\mathbf{T}_{(\cdot)}$ is diagonal with nonzero terms equal to the correlation time constants. As for $\gamma_{(\cdot)}$, it is characterized by its standard deviations; similarly for $\xi_{(\cdot)}$ above. The desired standard deviation of $\Delta\mathbf{v}_{(\cdot)}$ may be used together with $\mathbf{T}_{(\cdot)}$ to find the steady-state standard deviation of $\gamma_{(\cdot)}$.

C. Model Aiding

A DVL may or may not be part of the sensor suite, and even when it is, situations may arise where it fails to work or measurements are discarded due to reduced quality. For instance, this will occur when operating in the midwater zone, above the sensor range, or over rough bathymetry due to loss of bottom track. In the absence of DVL measurements, alternative velocity information is required to achieve an acceptable low drift INS solution between position updates. As for the acoustic positioning, it may be available often or only sporadically. Both types of measurements are essential for the INS performance, and as shown in Section IV-B, the solution from an INS without position and velocity aiding quickly becomes useless. This leads back to the questions addressed in this paper—Can the integration of a kinetic vehicle model improve the robustness, reliabil-

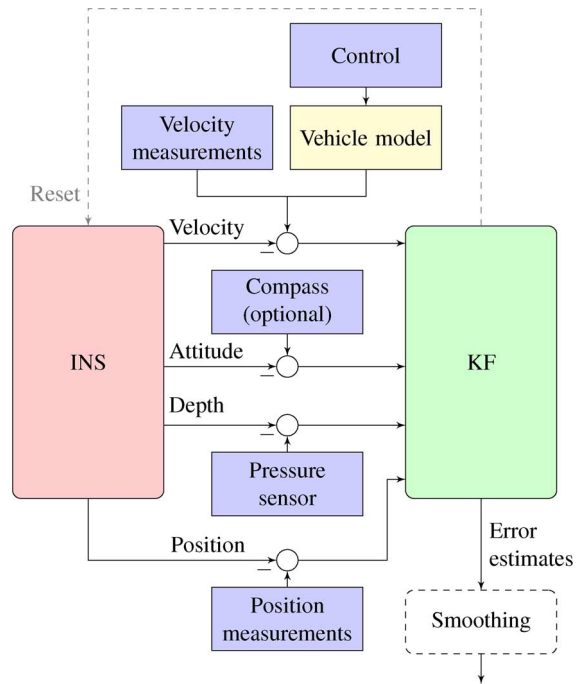


Fig. 7. Schematic diagram of the MA-INS (and conventional INS). External velocity measurements may be included in addition to the kinetic vehicle model. The addition of a DVL with bottom track and various operational scenarios are investigated in this work. The position measurements may be available often or only sporadically.

bility, and accuracy of an INS when: 1) DVL is available and the position measurements are received at various rates; 2) DVL is not available and the position measurements are received at various rates; 3) both position and DVL measurements become unavailable?

The basic idea and concept of using a kinetic vehicle model for aiding an INS is illustrated in Fig. 6(b), where the output from the model is treated analogously to that of an external aiding sensor. The MA-INS clearly resembles the conventional aided INS in Fig. 6(a), and both systems may share the same aiding sensors. A more detailed outline of the conventional INS and the MA-INS evaluated herein is shown in Fig. 7, differing only in the velocity aiding. It should be emphasized that the integration of a vehicle model in the navigation system does not require any additional sensors or instrumentation since the necessary inputs to the vehicle model for most vehicles are readily available whether model aiding is incorporated or not (i.e., actuation signals and vehicle roll and pitch). Furthermore, and as mentioned in Section II-D, the vehicle model may also be initialized independently of the current state of the INS or other external sensors.

It should also be pointed out that any vehicle model providing estimates of the position, attitude, or linear and angular velocity, may in principle be used as an INS aiding tool. For the position and attitude, in addition to the dynamics, one would have to extend the model to also include equations for the necessary kinematic relationships [38]. Unfortunately, this introduces one more integration, hence making the position and attitude states less suitable for aiding the INS. Contrary, one may argue that the linear and angular velocity states in kinetic models such as those

discussed in Section II-C will not drift but remain bounded for all practical inputs, i.e., measured and bounded actuation, and vehicle roll and pitch. This is a result of the dissipative properties of the models, per hydrodynamic damping. Since the velocity states are bounded it follows that the model output error is also bounded, that is, when compared to the actual or true linear and angular vehicle velocity. Velocity estimates from kinetic models are for the same reason tractable INS aiding measures.

1) Measurement and Process Equations: A DVL measures the vehicle velocity relative to the bottom, and is therefore unaffected by the sea current. In contrast, the velocity calculated by the kinetic vehicle model is relative to the water, hence to better make use of this velocity estimate for navigation purposes, the current must be accounted for.

Following along the same lines as in Section III-B, the error velocity related to the vehicle model is defined as

$$\delta z_{\text{vel}}^{\text{VM}} \triangleq z_{\text{vel}}^{\text{VM}} - \check{z}_{\text{vel}}^{\text{INS}}. \quad (47)$$

Furthermore, motivated by (10), the generalized linear velocity associated with the vehicle model and current is defined as

$$z_{\text{vel}}^{\text{VM}} \triangleq \check{v}_{\underline{e}w}^l + \check{R}_b^l \tilde{v}_{\underline{w}b}^b \quad (48)$$

where $\tilde{v}_{\underline{w}b}^b$ is the water-relative linear velocity provided by the vehicle model and $\check{v}_{\underline{e}w}^l$ is the calculated sea current velocity. As earlier, \check{R}_b^l stems from the INS. Substituting for the variables on the right-hand side of (47) gives the expression

$$\delta z_{\text{vel}}^{\text{VM}} = \check{v}_{\underline{e}w}^l + \check{R}_b^l \tilde{v}_{\underline{w}b}^b - \check{v}_{\underline{e}b}^l. \quad (49)$$

Note that the vehicle model output is treated as a measurement. It is obtained from measured actuation signals (propeller revolution and control surface deflections). Also note that if the current was measured it should be used in place of $\check{v}_{\underline{e}w}^l$.

In this paper, we assume that $\check{v}_{\underline{e}w}^l = 0$, which is to say that our best *a priori* guess of the current is zero. It does not mean that the true current is zero. As shown subsequently, the true current is estimated in the navigation system KF. Also, since the kinetic vehicle model does not include the water-relative velocity in heave as a state, the third entry of $\tilde{v}_{\underline{w}b}^b$ is defined to be zero. Similar to the sea current, the true water-relative heave velocity is estimated in the KF. The inclusion of a depth sensor in the navigation system renders this state observable.

Substituting with errors and true values in (49) yields

$$\delta z_{\text{vel}}^{\text{VM}} = (\check{v}_{\underline{e}w}^l + \delta v_{\underline{e}w}^l) + \delta R_b^l R_b^l (\tilde{v}_{\underline{w}b}^b + \delta v_{\underline{w}b}^b) - (\check{v}_{\underline{e}b}^l + \delta v_{\underline{e}b}^l) \quad (50)$$

where δR_b^l is the attitude deviation matrix, as described above. From the relationship in (10) and under the assumption of small orientation errors, (50) can be written to first order as

$$\delta z_{\text{vel}}^{\text{VM}} = \delta v_{\underline{e}w}^l + R_b^l \delta v_{\underline{w}b}^b - \delta v_{\underline{e}b}^l - S(\check{v}_{\underline{w}b}^b) e_{lb}^l. \quad (51)$$

The dependency to $\check{v}_{\underline{w}b}^b$ can be removed by applying (10) a second time and by recognizing that $\check{v}_{\underline{e}w}^l = -\delta v_{\underline{e}w}^l$, which follows from (41). The final expression for the measurement equa-

tion associated with the kinetic vehicle model and the sea current is given to first order as

$$\delta z_{\text{vel}}^{\text{VM}} = \delta v_{\underline{e}w}^l + R_b^l \delta v_{\underline{w}b}^b - \delta v_{\underline{e}b}^l - S(v_{\underline{e}b}^l) e_{lb}^l. \quad (52)$$

The latter equation clearly resembles the expression in (43). As in the DVL case, the best *a priori* estimates are used in place of R_b^l and $v_{\underline{e}b}^l$, calculated according to (44).

It is assumed herein that both the vehicle model output error $\delta v_{\underline{w}b}^b$ and the *a priori* current prediction error $\delta v_{\underline{e}w}^l$ can be modeled as the sum of colored noise and zero-mean white noise. The entries of both $\delta v_{\underline{w}b}^b$ and $\delta v_{\underline{e}w}^l$ are considered uncorrelated. If we let $\Delta v_{(\cdot)}$ and $\xi_{(\cdot)}$ denote the colored and white noises, respectively, the errors can be expressed as

$$\delta v_{\underline{w}b}^b = \Delta v_{\underline{w}b}^b + \xi_{v_{\underline{w}b}^b} \quad (53)$$

$$\delta v_{\underline{e}w}^l = \Delta v_{\underline{e}w}^l + \xi_{v_{\underline{e}w}^l}. \quad (54)$$

Since the velocity states in the vehicle model are obtained through integration there will be a sample to sample correlation. This is due to the inherent Markov property of the ODEs. The correlation may be accounted for through the choice of a suitable error-dynamics model. It is assumed in this paper that a first-order Markov model is adequate, and the colored noises in (53) and (54) are consequently implemented as zero-mean first-order Markov processes driven by white noise, that is

$$\dot{\Delta v}_{\underline{w}b}^b = -T_{\Delta v_{\underline{w}b}^b}^{-1} \Delta v_{\underline{w}b}^b + \gamma_{\Delta v_{\underline{w}b}^b} \quad (55)$$

$$\dot{\Delta v}_{\underline{e}w}^l = -T_{\Delta v_{\underline{e}w}^l}^{-1} \Delta v_{\underline{e}w}^l + \gamma_{\Delta v_{\underline{e}w}^l}. \quad (56)$$

The colored noises are states in the KF process equation. Also recall that the estimate of $\Delta v_{\underline{e}w}^l$ is also an estimate of $\delta v_{\underline{e}w}^l$. Negated, this is again an estimate of the true sea current.

Note that as pointed out in Section III-B, many alternative correlation models exist. A popular model is that of random walk (RW), which is equivalent to the first-order Markov model as the time constant T approaches infinity. A drawback of the RW is that the prediction uncertainty grows unbounded with time, as opposed to the first-order Markov model where it is possible to specify the desired steady-state uncertainty. Since the vehicle model output error is bounded the Markov model yields a more physical interpretation. The use of alternative correlation models is not discussed any further in this paper.

2) Measurement and Process Noise Level Switching: The parameters describing the errors in the aiding sensors are time invariant by default. However, for some sensors, explicit knowledge of the measurement accuracy degradation or improvement from one sample to another may be available, e.g., through quality numbers reported by the sensor itself. If feasible, the quality of each single measurement should be incorporated in the KF. Typically, the resulting effect is an increase or decrease in the measurement white noise, and in some cases, a change in the standard deviation or correlation time constant for the colored noise. In this work, the USBL measurements are accompanied by distinct quality measures at each sample, as reported by the sensor.

Analogous to a conventional aiding sensor, the vehicle model output varies in quality. In particular, the accuracy during tight

turning maneuvers is slightly lower than for steady forward motion, as experimentally validated in [26]. In [8], the normalized innovation is monitored to detect a maneuver, and if it exceeds a certain threshold the KF process noise is adjusted. A related approach is applied in this paper for adjusting the process and measurement noise characteristics associated with the vehicle model output error δv_{wb}^b . However, in contrast to the systems in [8], a maneuver for an underwater vehicle is detected directly from the measured actuation. This knowledge may be used for establishing a noise level switching rule. An outline of the rule used in this paper is given in Algorithm 1. While not considered in this work, a similar criterion can easily be developed for stern plane deflections and vertical or coordinated maneuvers.

Algorithm 1: Trajectory-based noise level switching

Input Rudder deflection angle τ [$^\circ$]
Output Adjusted KF noise characteristics for δv_{wb}^b

if $|\tau| >$ threshold **then**

adjust appropriate entries of T , γ and ξ

else

t : time since $|\tau| >$ threshold

if $t <$ settle time **then**

adjust appropriate entries of T , γ , ξ

else

reset T , γ , ξ to nominal values

D. Practical Considerations

The success of MA-INS evidently depends on the fidelity of the kinetic vehicle model, as well as the ability of the integrated navigation system to estimate environmental disturbances, in this case sea current. At the same time, it is well known that an INS without sufficient aiding rapidly drifts off in both position and velocity, as illustrated in Section IV. Depending on the IMU class, the error and uncertainty of the INS velocity quickly become larger than the combined sea current estimation error and output error of the kinetic vehicle model. Recall that an INS based on a navigation grade IMU drifts in the order of 1 nmi/h if left unaided. This corresponds to an average INS speed error of about 0.5 m/s. While a general analysis of vehicle model fidelity versus IMU class is not included in this paper, this indicates that even less accurate models may be utilized as aiding tools and hence reducing the otherwise inevitably INS position drift. The effort needed for developing a model that is suitable for aiding the INS is moderate, and the main involvement is to obtain data for the parameter identification task and model validation. An important observation is that these data often are already available from earlier sea trials or they may be gathered indirectly as part of other tests or future missions. Another important observation is that the effort is nonrecurring, that is, once the model has been developed it may be utilized as an aiding tool on any other vehicle having the same particulars and hydrodynamics.

It should also be pointed out that while the use of a kinetic vehicle model successfully restrains the INS velocity error growth, it cannot bound the position error drift indefinitely.

This is the case for any velocity measurements having some form of bias, including those obtained from DVL. As for MA-INS, the navigation accuracy obtained during time periods without position and DVL aiding is limited to the accuracy of the estimated sea current and vehicle model output error. If the current and model accuracy do not change significantly during these time slots, the navigation accuracy will remain good. As shown in Section IV-B, the MA-INS maintains a respectable accuracy even after one hour with position and DVL aiding absent. The alternative to run the INS without model aiding in these cases rapidly becomes useless. Note that as with any navigation system, the feasible operating time is limited by the required accuracy. As shown subsequently, the MA-INS can provide a standalone navigation system as long as position or DVL measurements are provided at a frequency necessary to keep the navigation solution within some desired accuracy. While not discussed any further in this paper, note also that the output from the 3-DOF vehicle model may be integrated in time together with external attitude data to provide a secondary dead-reckoning position. This may be useful for emergency navigation in the rare case of IMU failure. The navigation performance when using the vehicle model alone will typically be significantly lower than for the MA-INS due to the lack of embedded compensation of model output error and sea current. The difference between the two approaches evidently depends on the fidelity of the model and the magnitude of the current.

The 3-DOF kinetic model used for aiding the INS in this paper was derived with the assumption of negligible coupling from velocity in heave, and angular rates in roll and pitch. These are reasonable assumptions for AUVs navigating in the geographical horizontal plane, possibly subject to small adjustments in pitch and low-rate depth changes. This is representative for normal operations with the HUGIN AUV considered herein. While additional states could have been used for aiding the INS, the velocity components in surge and sway are particularly important when considering navigation in the geographical horizontal plane. Recall also that the depth sensor efficiently pins down the vertical position error drift.

While not considered in this paper, a 3-DOF kinetic model with surge, heave, and pitch rate as states could have been used for modeling the vehicle motion more accurately during steep ascents or descents, typically carried out at the start and end of a mission. The INS aiding methodology remains the same as in the horizontal case, including the use of adaptive noise level switching rules as described earlier. Higher DOF models should be considered for strongly coupled and coordinated maneuvers. In general, the more accurate the kinetic vehicle model is the better it is suited for aiding the INS. However, as mentioned, the necessary accuracy depends on the expected short- and long-term free-inertial drift of the INS velocity, and evidently, the required accuracy of the final MA-INS solution.

As for some final considerations, it should be mentioned that the sea current and model output error are only observable during time periods with either position or DVL measurements. For operations where neither will be available for considerable time, e.g., covert or entirely autonomous operations, or where the risk of outage is substantial, it is important that the MA-INS is properly initialized in advance. It is furthermore seen from



Fig. 8. The HUGIN 4500 AUV during sea trial launch in October 2006.

TABLE II
IMU SPECIFICATIONS

Model	Gyro Technology	Gyro Bias	Accelerometer Bias	Rate
IXSEA IMU90	Fiber optic	$\pm 0.05 \text{ deg/h}$	$\pm 500 \mu\text{g}$	100 Hz

(52) that the sea current and model output error are only separable through the rotation matrix \mathbf{R}_b^l . In the horizontal case, this signifies that heading changes are required to distinguish between the two. In the case of constant sea current and constant water-relative vehicle velocity (both unknown), it was found in [26] and [34] that only few heading changes were necessary to make the analogously LS estimation problem well posed, that is, to make the sea current and water-relative vehicle velocities observable.

IV. FIELD EXPERIMENTS

The performance and comparison of the MA-INS and the conventional INS are evaluated on experimental data collected by the HUGIN 4500 vehicle, a field-deployed AUV designed for underwater surveying and mapping. An overview of the experimental setup, including employed navigation sensors, vehicle trajectories, and the processing of raw navigation data, is given in Section IV-A. The experimental results and comparative evaluation are presented in Sections IV-B and IV-C. The performance of the navigation system with and without model aiding included is of particular interest.

A. Experimental Setup

1) *Vehicle Description:* The HUGIN 4500 is the largest member of the Kongsberg Maritime HUGIN AUV family. The surface ship, the launch and recovery system, and the AUV are shown in Fig. 8. The diameter and length of the vehicle are 1 and 6.5 m. The vehicle with full payload can operate for 60–70 h at depths down to 4500 m, at a cruising speed of about 1.9 m/s. The vehicle is passively stable in roll and close to neutrally buoyant. For propulsion, it is fitted with a single three-bladed propeller. A cruciform tail configuration with four identical control surfaces is used for maneuvering.

TABLE III
PRIMARY NAVIGATION AIDING SENSORS

Variable	Sensor	Accuracy/Precision	Rate
Position	Kongsberg HiPAP	Range, Angle: < 20 cm, 0.12 deg	Varying*
Velocity	RDI 300kHz DVL	$\pm 0.4\% \pm 0.2 \text{ cm/s}$	1 Hz
Pressure	Paroscientific	0.01 % full scale	1 Hz

* Stored topside at approximately 1/3 Hz. While submerged, the AUV receives position updates at about 1/30 Hz, from the surface via an acoustic link.

Logged from 06-Oct-2006 05:01:09 to 06-Oct-2006 07:14:14

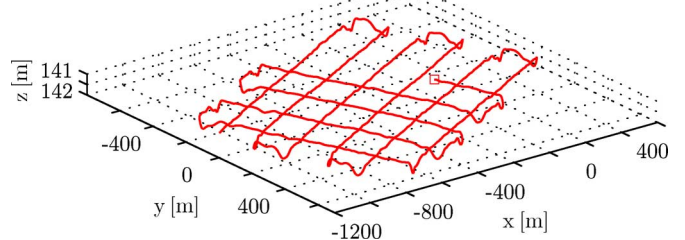


Fig. 9. Vehicle lawn-mower trajectory. The trajectory shows the RTS smoothed local vehicle position \mathbf{p}_{mb}^m , obtained from the USBL-DVL-INS using the highest sensor update rates available. This solution is considered as ground truth when evaluating the MA-INS and the case scenarios herein.

HUGIN 4500 is equipped with a conventional aided INS, as outlined in Fig. 7. Some IMU specifications are listed in Table II. A surface ship tracks the AUV with a USBL acoustic positioning system. By combining DGPS with USBL, a global position estimate can be obtained, which is then transmitted to the AUV. Additional navigation sensors include compass (optional and only included for redundancy since the system incorporates a considerably more accurate IMU), pressure sensor, and DVL with bottom track. Primary sensors and some of their specifications are listed in Table III. For further information on the navigation system and the navigation system accuracy, the reader may refer to [10], [47], and [52].

2) *Experimental Description:* In September and October 2006, several sea trials were conducted with HUGIN 4500 near $59^\circ 29'N$, $10^\circ 28'E$, in the Oslo-fjord, Norway. Roughly 60 h of data were collected, of which a subset of about 5 h was utilized during the model development and cross validation. Another 4 h are utilized in this paper for evaluating the navigation system. In the first part of the data, the vehicle was kept at a constant depth while moving along square-shaped trajectories, as described in [34]. In the second part, the vehicle followed a standard lawn-mower pattern, typical for a survey AUV. The vehicle trajectory corresponding to the latter data is shown in Fig. 9. For all the data utilized in this work the vehicle depth and height above the seabed were in the order of 130–160 and 40–70 m, respectively.

3) *Data Postprocessing:* Raw sensor values (without any filtering) are used throughout this paper for the DVL velocities, pressure readings, and IMU angular rates and specific forces. Similarly, raw actuator signals are used for generating the vehicle model measurements. The USBL position data were inspected and outliers removed. The HUGIN 4500 navigation system then reprocessed the appropriate sensor data to get real-time estimates from the KF (this is done using a duplication of the vehicle at-sea navigation system, also integrating model aiding and sea current estimation). The renavigation

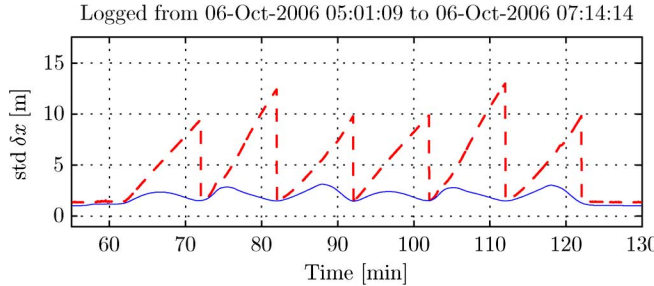


Fig. 10. Effectiveness of doing RTS smoothing. The estimated smoothed and real-time north position uncertainties (1σ) are shown in blue (solid) and red (dashed), respectively. The data correspond to Case 2-5 in Section IV-B.

routines and postprocessing framework are implemented in NavLab [47], a tool which has been used extensively with all the HUGIN AUVs since the late 1990s.

In addition to renavigating the HUGIN real-time navigation system, NavLab also contains offline smoothing functionality, based on a Rauch–Tung–Striebel (RTS) implementation. The RTS smoother utilizes both past and future sensor measurements and KF covariances, hence efficiently improving the integrity and accuracy of the final navigation solution. An example illustrating the effectiveness of smoothing is shown in Fig. 10. In this paper, the smoothed USBL-DVL-INS solution with the highest navigation sensor update rates available serves as the basis or reference when evaluating the performance of the MA-INS and the different scenarios reported in this work. The accuracy of the RTS smoothed basis position was estimated to be 0.75 m (1σ) in north and east. Additional information on the experimentally proven accuracy of the smoothed navigation solution may be found in [47].

B. Experimental Results

This section evaluates the performance of the MA-INS and conventional INS described in Section III. All the KF tuning parameters common to the MA-INS and the conventional INS are equal throughout this paper. The parameters associated with the vehicle model and sea current are also identical in all the considered scenarios. Unless mentioned otherwise, the position measurements are received regularly at about 1/3 Hz, and when applicable, the vehicle model output and DVL measurements are processed at 1 Hz. As mentioned in Section IV-A3, the RTS smoothed basis solution serves as the ground truth during comparison. Unless stated otherwise, the evaluation of the navigation system and scenario in discussion is based on the real-time KF solution and its predicted estimation uncertainties. An estimation error is taken as the difference between the basis or reference solution and the solution from the integrated navigation system being evaluated.

1) Estimation of Sea Current and Vehicle Model Output Error in MA-INS: The ability to estimate sea current in both real time and postprocessing is of great importance when utilizing a navigation sensor that measures the vehicle velocity relative to the water. Any bias in the estimated sea current yields, if DVL and position measurements are absent, a direct position error drift

TABLE IV
REAL-TIME SEA CURRENT ESTIMATION DURING SQUARE MANEUVERS

Square	Estimation approach	Log time	$\ \mathbf{v}_{ew}^l\ $	β_w
1	LS from [34]	Oct 06 @ 02:06-02:20	0.015	17.2
	DVL-MA-INS	Oct 06 @ 02:03-02:20	0.012	32.1
	USBL-MA-INS	Oct 06 @ 02:03-02:20	0.010	35.3
	USBL-DVL-MA-INS	Oct 06 @ 02:03-02:20	0.012	35.4
2	LS from [34]	Oct 06 @ 03:01-03:21	0.018	305.5
	DVL-MA-INS	Oct 06 @ 03:01-03:21	0.017	311.9
	USBL-MA-INS	Oct 06 @ 03:01-03:21	0.017	318.6
	USBL-DVL-MA-INS	Oct 06 @ 03:01-03:21	0.018	312.8
3	LS from [34]	Oct 06 @ 04:15-04:34	0.004	301.7
	DVL-MA-INS	Oct 06 @ 04:06-04:34	0.007	310.6
	USBL-MA-INS	Oct 06 @ 04:06-04:34	0.006	306.9
	USBL-DVL-MA-INS	Oct 06 @ 04:06-04:34	0.007	310.3
4	LS from [34]	Oct 06 @ 07:31-07:46	0.021	162.7
	DVL-MA-INS	Oct 06 @ 07:26-07:48	0.018	160.4
	USBL-MA-INS	Oct 06 @ 07:26-07:48	0.018	150.7
	USBL-DVL-MA-INS	Oct 06 @ 07:26-07:48	0.018	159.5

in north and east. Besides being used for navigation, a sea current estimate may be of interest for other applications as well, e.g., oceanography and marine research, and autonomous mission planning and decision making.

The magnitude or speed of the estimated current is taken as the Euclidian norm of \mathbf{v}_{ew}^l . It is assumed throughout this work that the vertical current component, or equally, the third entry of \mathbf{v}_{ew}^l is negligible. Recall that the negated estimate of $\delta\mathbf{v}_{ew}^l$ also yields an estimate of the true sea current \mathbf{v}_{ew}^l . The sea current direction β_w is calculated from

$$\beta_w = \text{atan2}(\mathbf{v}_c^l, u_c^l) \quad (57)$$

where $\beta_w \in [0, 360]$ is relative north with positive rotation clockwise, i.e., $\beta_w = 90^\circ$ equals east direction.

The estimated current speeds and directions resulting from four horizontal square-like trajectories are summarized in Table IV. The estimates from the MA-INS are compared to the LS results reported in [34]. The two conceptually different approaches show good agreement. The USBL-MA-INS real-time and smoothed KF evolutions for square 3 and 4 are shown together with the corresponding LS solutions in Fig. 11. The DVL-MA-INS and the USBL-DVL-MA-INS show a similar behavior, with the latter having slightly quicker convergence rate than the first two. Recall that it is not possible to estimate the sea current in the case where both DVL and USBL are unavailable. The MA-INS values in Table IV are taken as the median of the last 8 min of the real-time KF time sequences.

Since the heave velocity from the vehicle model is zero by assumption, it follows from (41) that the KF estimate of $\delta v_{wb,z}^b$ also yields an estimate of w_r . The estimated USBL-MA-INS water-relative heave velocity for square 1 is shown in Fig. 12. Similar results are obtained for the other data in this paper as well. The good observability is due to the inclusion of a depth sensor in the navigation system sensor suite. The observability is further increased when including the DVL. The MA-INS also estimates the surge and sway components of δv_{wb}^b . Both were estimated to be a few centimeters per second or less during steady forward motion, and slightly higher during the turns, as anticipated and discussed in Section III-C2.

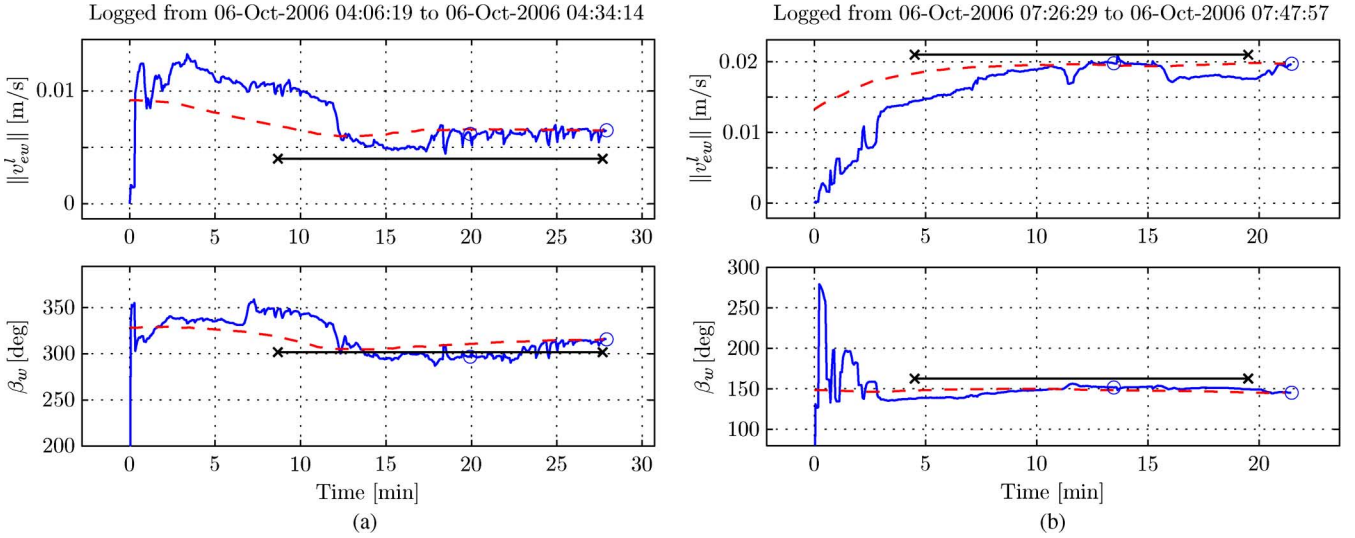


Fig. 11. Estimated current using LS [34] and MA-INS: (a) Current for square 3 in Table IV. The USBL-MA-INS real-time and smoothed KF estimates are shown in blue (solid) and red (dashed), respectively. The black (x-x) lines are the corresponding LS solutions. (b) Current for square 4 in Table IV. Similar labels as in (a). The MA-INS values in Table IV are taken as the median of the last 8 min of the real-time KF estimates, indicated with blue “o.”

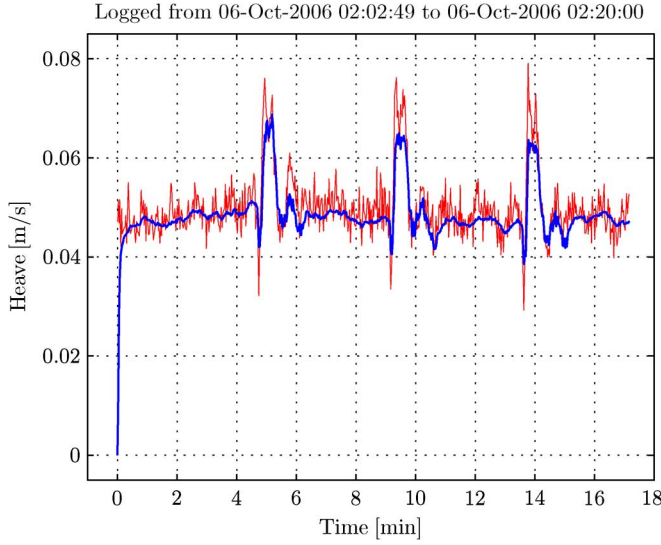


Fig. 12. Vehicle water-relative heave velocity for square 1. The blue (solid) is the USBL-MA-INS estimate of w_r and the red (dashed) is the ground truth w . From (10), it is straightforward to verify that w and w_r will be approximately equal for zero vertical current and small roll and pitch angles.

As mentioned, the MA-INS performance partly depends on the ability to estimate the sea current and the model output error. From the relationships in (10) and (41), we get that

$$\underline{v}_{eb}^b = \mathbf{R}_l^b \left(\underline{v}_{ew}^l - \delta \underline{v}_{ew}^l \right) + \left(\tilde{\underline{v}}_{wb}^b - \delta \underline{v}_{wb}^b \right). \quad (58)$$

Based on the expression in (58), one can calculate the Earth-relative velocity resulting from the kinetic vehicle model output and the KF estimates of the sea current and model output error. Recall that \underline{v}_{ew}^l is assumed zero herein. The difference between the surge and sway components of the velocity found in (58) and the equivalent basis velocity is shown in Fig. 13. The data correspond to square 2 and the DVL-MA-INS solution. The basis

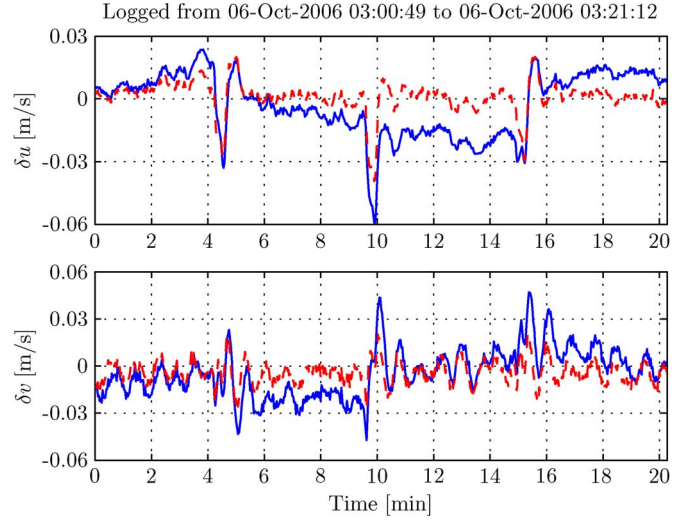


Fig. 13. Difference between the surge and sway components of the velocity found in (58) and the equivalent basis velocity. Data shown for square 2 in Table IV and DVL-MA-INS. The blue (solid) lines are obtained from using the model output directly without error compensation. The red (dashed) lines also incorporate KF estimates of the model output error and sea current.

attitude data were used for calculating \mathbf{R}_l^b . Overall, the two velocities show good agreement, indicating that the combined estimation error of the sea current and model output error is low. Similar results are obtained for the other squares and data in this paper as well, and for the USBL-MA-INS and the USBL-DVL-MA-INS. Note that the increased error or differences occurring during the turns are accounted for in the KF covariance per Algorithm 1. This is illustrated for the lawn-mower-type data in Fig. 14.

2) *Sparse or Reduced Frequency Position Updates in USBL-INS and USBL-MA-INS:* This experiment was done to evaluate the performance of the integrated INS in cases where measurements from a DVL are nonexistent and position measurements are sparse or for some reason become unavailable

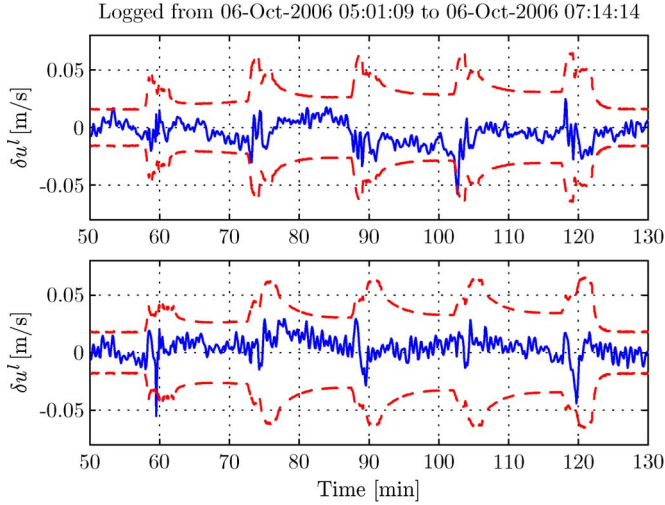


Fig. 14. North and east velocity errors and uncertainties. The blue (solid) data show the north and east velocity errors for the USBL-MA-INS, according to Case 2-8. The corresponding KF real-time uncertainties (1σ) are shown in red (dashed). The distinct increase in the uncertainties occurs during the turns, and is due to adjusted process and measurement noise, per Algorithm 1.

for extended periods of time. The lack of DVL measurements will certainly be the case when operating in the midwater zone, above the DVL sensor range. It may also be due to system failure, or simply, if no DVL unit is included in the navigation system sensor suite. Having a low position update rate is often the situation in entirely autonomous operations. Also, when covering large areas, the vehicle may temporarily operate outside the range of the acoustics positioning; either this is facilitated by a surface ship located within some boundary of the survey area, from a long baseline (LBL) grid, or from one or several underwater transponder positioning (UTP) transponders [10], [53]. Note that while only considering USBL positioning in this paper, the results and analysis are applicable to other systems as well, including the use of GPS surface fix. Note also that even when acoustic positioning is available, the update frequency may be limited by the bandwidth of the acoustic link or due to possible interference from other components. The INS will in either case chiefly depend on velocity aiding to retain an acceptable low drift navigation solution between position updates. As discussed shortly, the performance of the INS without velocity aiding from the kinetic vehicle model quickly deteriorates as the position update frequency goes down.

The scenarios investigated in this section are best described from Fig. 15, where the navigation system receives position measurements regularly at about 1/3 Hz for about 62 min. The position measurements are then decimated or completely removed for the next 60 min. The decimation is carried out for several frequencies, ranging from 1/30 Hz to a complete outage. The latter example is shown in Fig. 15. The different conditions and scenarios are summarized in Table V, where the experiments labeled Case 1 and Case 2 denote the INS results without and with model aiding, respectively. Note that no modifications are made to the USBL data except for removing raw samples to obtain the desired frequency. Starting from 122 min and for the remainder of the survey, the position measurements are again received at a regular rate.

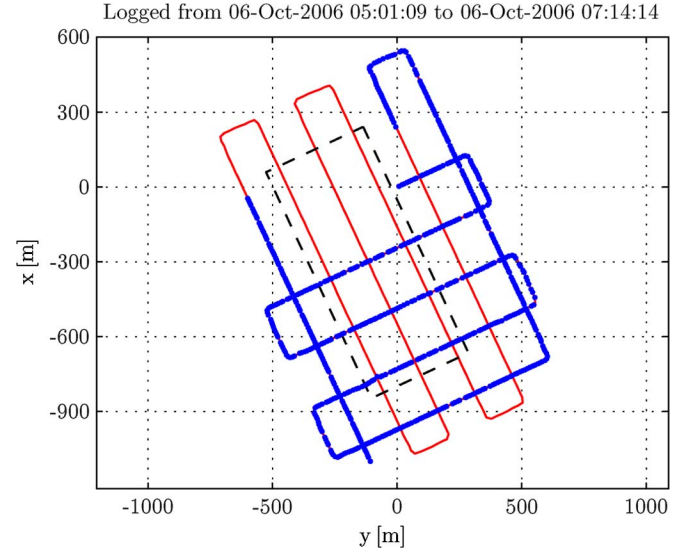


Fig. 15. The red (solid) trajectory is the horizontal basis position, with its initial location at the origin. The blue “o” data show the position measurements logged at about 1/3 Hz. The segment without position measurements corresponds to 60 min, occurring between 62 and 122 min into the survey. The dashed rectangle applies to the scenarios in Section IV-B4, where the DVL measurements become unavailable when operating within this area.

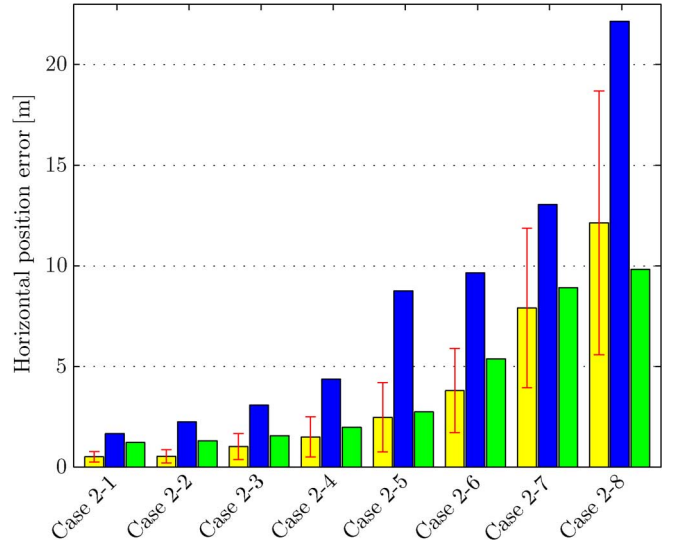


Fig. 16. Horizontal position estimation errors for Case 2 in Table V: The bars from left to right show the mean and standard deviation of the real-time USBL-MA-INS position error, the maximum real-time USBL-MA-INS position error, and the maximum RTS smoothed USBL-MA-INS position error.

As can be seen from the results summarized in Table V, the navigation performance of the USBL-MA-INS is superior to that obtained with the conventional USBL-INS. The values in the table are for the interval between 62 and 122 min. As anticipated, the significance of incorporating model aiding in the navigation system becomes increasingly apparent as the position update frequency decreases. The difference in performance is significant also at the highest update rates. While the conventional USBL-INS is sensitive to the position update rate, the USBL-MA-INS is considerably more robust and is able to keep the sustainability and accuracy of the navigation system at a satisfactory level even during long time periods without position measurement updates. A subset of

TABLE V
SUMMARY OF EXPERIMENTS AND RESULTS: THE VALUES ARE REPRESENTATIVE FOR THE TIME INTERVAL BETWEEN 62 AND 122 MIN

Experiment	Time between updates			Position error within 1σ		Horizontal position error			Smoothed horizontal position error		
	USBL	DVL	VM	North (x)	East (y)	max	mean	std	max	mean	std
Case 1-1	30 s	-	-	100.00%	100.00%	2.78 m	0.54 m	0.32 m	0.85 m	0.41 m	0.16 m
Case 2-1	30 s	-	1 s	100.00%	100.00%	1.66 m	0.51 m	0.26 m	1.22 m	0.42 m	0.21 m
Case 3-1	30 s	1 s	-	100.00%	100.00%	0.76 m	0.32 m	0.13 m	0.05 m	0.02 m	0.01 m
Case 4-1	30 s	1 s	1 s	100.00%	100.00%	0.85 m	0.31 m	0.13 m	0.18 m	0.09 m	0.04 m
Case 1-2	60 s	-	-	100.00%	100.00%	4.63 m	0.84 m	0.63 m	1.07 m	0.38 m	0.18 m
Case 2-2	60 s	-	1 s	100.00%	100.00%	2.24 m	0.53 m	0.33 m	1.31 m	0.43 m	0.21 m
Case 3-2	60 s	1 s	-	100.00%	100.00%	0.75 m	0.34 m	0.15 m	0.05 m	0.03 m	0.01 m
Case 4-2	60 s	1 s	1 s	100.00%	100.00%	0.82 m	0.33 m	0.13 m	0.15 m	0.08 m	0.04 m
Case 1-3	180 s	-	-	100.00%	100.00%	53.93 m	9.65 m	9.00 m	1.30 m	0.52 m	0.26 m
Case 2-3	180 s	-	1 s	100.00%	100.00%	3.08 m	1.02 m	0.64 m	1.56 m	0.53 m	0.30 m
Case 3-3	180 s	1 s	-	100.00%	100.00%	1.15 m	0.42 m	0.19 m	0.20 m	0.07 m	0.05 m
Case 4-3	180 s	1 s	1 s	100.00%	100.00%	0.86 m	0.41 m	0.18 m	0.23 m	0.10 m	0.05 m
Case 1-4	300 s	-	-	100.00%	100.00%	229.22 m	36.69 m	41.56 m	4.61 m	1.58 m	1.03 m
Case 2-4	300 s	-	1 s	100.00%	100.00%	4.37 m	1.50 m	1.00 m	1.97 m	0.59 m	0.41 m
Case 3-4	300 s	1 s	-	100.00%	100.00%	1.63 m	0.56 m	0.31 m	0.27 m	0.15 m	0.06 m
Case 4-4	300 s	1 s	1 s	100.00%	100.00%	1.26 m	0.48 m	0.27 m	0.23 m	0.12 m	0.06 m
Case 1-5	600 s	-	-	100.00%	100.00%	953.11 m	185.69 m	224.10 m	16.81 m	7.26 m	5.12 m
Case 2-5	600 s	-	1 s	100.00%	100.00%	8.76 m	2.47 m	1.72 m	2.75 m	1.19 m	0.64 m
Case 3-5	600 s	1 s	-	100.00%	100.00%	2.73 m	0.96 m	0.60 m	0.72 m	0.40 m	0.16 m
Case 4-5	600 s	1 s	1 s	100.00%	100.00%	2.33 m	0.84 m	0.48 m	0.60 m	0.31 m	0.15 m
Case 1-6	1200 s	-	-	100.00%	100.00%	1838.97 m	567.75 m	568.10 m	108.97 m	41.68 m	32.19 m
Case 2-6	1200 s	-	1 s	100.00%	100.00%	9.65 m	3.80 m	2.09 m	5.38 m	2.73 m	1.49 m
Case 3-6	1200 s	1 s	-	100.00%	99.83%	4.84 m	1.70 m	1.18 m	1.84 m	0.84 m	0.43 m
Case 4-6	1200 s	1 s	1 s	100.00%	100.00%	3.89 m	1.45 m	0.86 m	1.15 m	0.56 m	0.28 m
Case 1-7	1800 s	-	-	100.00%	100.00%	1734.42 m	435.63 m	381.67 m	732.92 m	265.01 m	229.29 m
Case 2-7	1800 s	-	1 s	100.00%	100.00%	13.05 m	7.90 m	3.96 m	8.91 m	3.83 m	2.30 m
Case 3-7	1800 s	1 s	-	100.00%	100.00%	3.98 m	2.15 m	0.82 m	3.28 m	1.28 m	0.84 m
Case 4-7	1800 s	1 s	1 s	100.00%	100.00%	4.33 m	1.84 m	0.88 m	2.35 m	0.91 m	0.55 m
Case 1-8	-	-	-	100.00%	100.00%	2208.49 m	897.33 m	684.00 m	1322.12 m	439.64 m	453.57 m
Case 2-8	-	-	1 s	100.00%	100.00%	22.15 m	12.13 m	6.56 m	9.83 m	5.45 m	2.43 m
Case 3-8	-	1 s	-	100.00%	100.00%	5.49 m	2.92 m	1.12 m	3.40 m	1.34 m	0.88 m
Case 4-8	-	1 s	1 s	100.00%	100.00%	5.69 m	2.88 m	1.28 m	2.58 m	1.15 m	0.57 m
Case 5-1	1800 s	★1 s	-	100.00%	100.00%	237.07 m	29.90 m	42.29 m	15.23 m	4.24 m	5.20 m
Case 5-2	1800 s	★1 s	1 s	100.00%	100.00%	7.48 m	2.48 m	1.71 m	2.73 m	1.01 m	0.69 m
Case 5-3	-	★1 s	-	100.00%	100.00%	256.75 m	35.04 m	44.41 m	13.09 m	5.35 m	4.60 m
Case 5-4	-	★1 s	1 s	100.00%	100.00%	7.48 m	4.27 m	2.12 m	3.51 m	1.79 m	1.00 m

* The DVL measurements are received regularly with exception of three distinct outages (each about 10 min), as illustrated in Figs. 1 and 15.

Case 2 results in Table V is highlighted in Fig. 16. Additional examples are shown in Fig. 17 for Cases 1-5 and 2-5, and in Fig. 18 for Cases 1-2 and 2-2. The north and east INS position errors are for all cases consistent with the KF covariances and within 1σ throughout. Similar results were obtained for the other experiments as well, all showing a significant better performance of the USBL-MA-INS than the USBL-INS. In the worst case, when operating for 1 h without position aiding, the maximum error of the USBL-INS is in the order of 2200 m. In the same scenario, the real-time USBL-MA-INS horizontal position error is confined within 22 m. The accuracy may be further enhanced by doing RTS smoothing, in which case the maximum error reduces to less than 10 m. The real-time north and east velocity errors and uncertainties for the same case scenario are shown in Fig. 14. The increased velocity uncertainty associated with the vehicle model output during the turns is accounted for in the KF covariances. The MA-INS velocity errors are consistent with the predicted uncertainties. A similar 1σ consistency is obtained for all the other cases as well, also for those not incorporating model aiding.

Another illustration of the effectiveness of including model aiding in the navigation system is shown in Fig. 18. As can be seen, the USBL-INS and the USBL-MA-INS provide very dif-

ferent position covariance estimates, and the uncertainties obtained by the latter system are clearly reduced. Similarly, the uncertainty growth in between position measurements is lowered significantly. As before the importance becomes increasingly apparent as the position update frequency decreases. The effect is also seen when receiving position measurements at higher update rates. When received at 1/3 Hz, the USBL-INS and the USBL-MA-INS perform comparably, with a slight advantage to the system with model aiding. However, as discussed above, the USBL-MA-INS is significantly more robust to even short position measurement dropouts. An acoustic positioning system is apt to lose transmission signals at some point, potentially leading to mission failure if not including satisfactory redundancy, for instance, model aiding.

3) *Sparse or Reduced Frequency Position Updates in USBL-DVL-INS and USBL-DVL-MA-INS:* This experiment was done to evaluate the performance of the integrated INS in cases where measurements from a DVL are received at a regular rate but position measurements are sparse or for some reason become unavailable for extended periods of time. This is a typical scenario for fully autonomous or covert operations in unknown areas, and in both civilian and military applications where the AUV is required to stay submerged for long periods of time. The solution

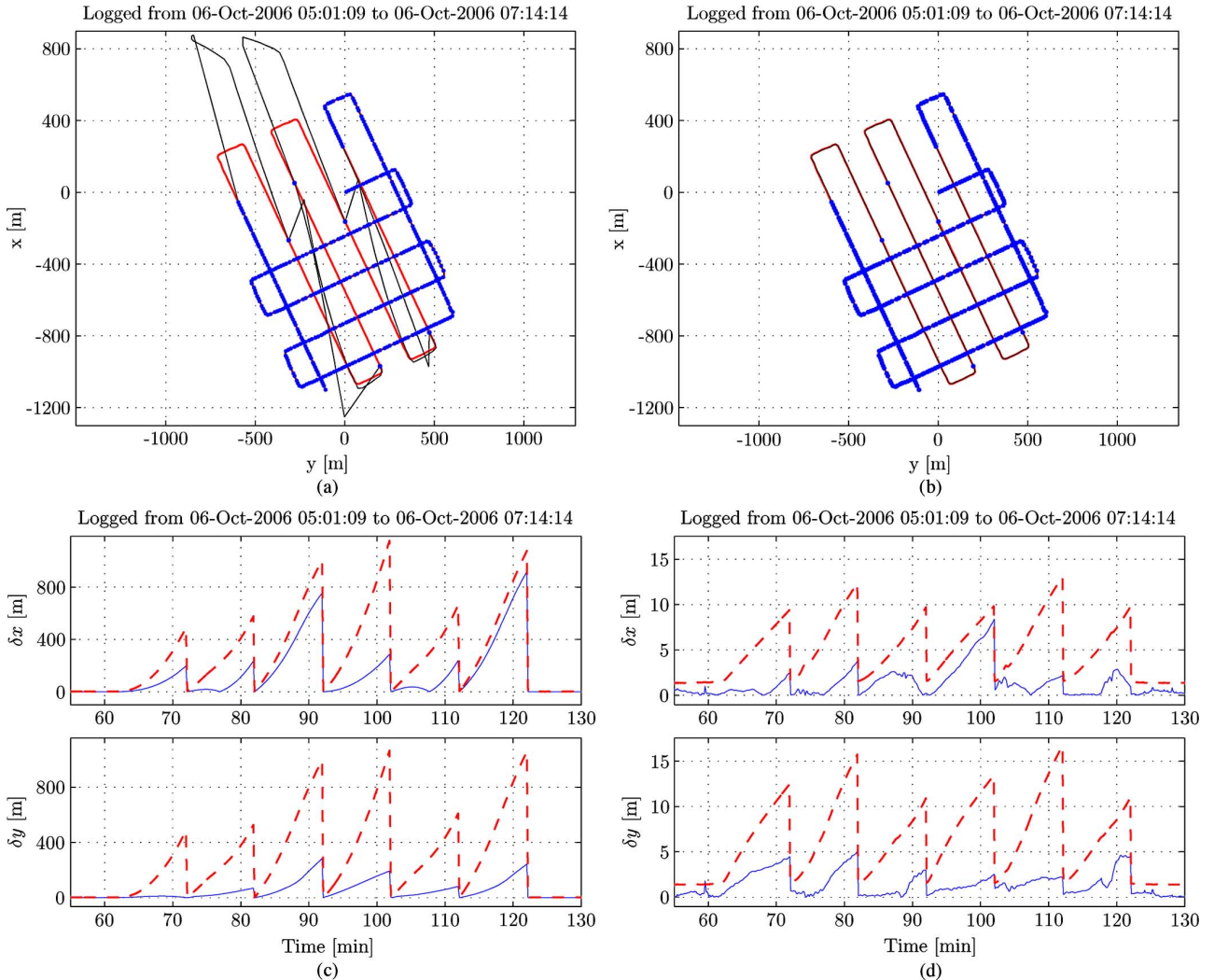


Fig. 17. Examples of USBL-INS and USBL-MA-INS performance with sparse or reduced frequency position updates: (a) The red (solid) trajectory is the horizontal basis position, with its initial location at the origin. The blue “o” data show the position measurements. The total length of the segment with reduced position update frequency is 60 min, occurring between 62 and 122 min into the survey. In the considered example, the position measurements in this interval are received at about 1/600 Hz, according to Case 1-5 in Table V. The real-time navigation solution obtained with the USBL-INS is shown in black (solid). (b) Similar labels and position measurements as in (a) but for USBL-MA-INS according to Case 2-5. The performance is significantly better than in the system without model aiding. (c) The blue (solid) data show the absolute value of the north and east position errors for the USBL-INS, according to Case 1-5. The corresponding KF real-time uncertainties (1σ) are shown in red (dashed). (d) Similar labels as in (c) but for USBL-MA-INS, according to Case 2-5.

for most modern AUVs is to utilize a DVL to limit or reduce the position error drift.

When operated within its range, the 300-kHz DVL considered herein provides Earth-relative velocity measurements at about $\pm 0.4\%$ of speed along all axes. In surge this corresponds to about 0.8 cm/s at 2 m/s forward speed. An interesting and relevant question is whether the incorporation of model aiding in the navigation system further enhances the precision obtained by the already accurate USBL-DVL-INS. Without the addition of DVL bottom-track measurements, all the circumstances and position update frequency scenarios are identical to those examined in Section IV-B2. The various conditions and results are summarized in Table V, where the experiments labeled Case 3 and Case 4 denote the integrated INS without and with model aiding included, respectively.

As can be seen from Table V, the navigation performance of the USBL-DVL-MA-INS is comparable or better than the USBL-DVL-INS throughout, and in both real time and when

running RTS smoothing. The north and east INS position errors are for all cases consistent with the KF covariances and well within 1σ . Similar consistency is found for the velocity errors as well. A subset of the Cases 3 and 4 results are highlighted in Fig. 19. While the impact of including model aiding is less striking than in the system not having DVL, the improvement achieved by the USBL-DVL-MA-INS is clearly visible. It should be kept in mind that the uncertainty associated with the DVL is significantly lower than the combined uncertainty of the vehicle model output and sea current. The performance enhancement is hence considered respectable. As discussed subsequently, and perhaps more importantly than the obtained accuracy gain, is the significant robustness and sustainability improvement of the MA-INS. For completeness note that the DVL was accurately aligned prior to collecting the at-sea data utilized in this work.

4) *DVL Outage and Sparse Position Updates in USBL-DVL-INS and USBL-DVL-MA-INS:* This experiment was done

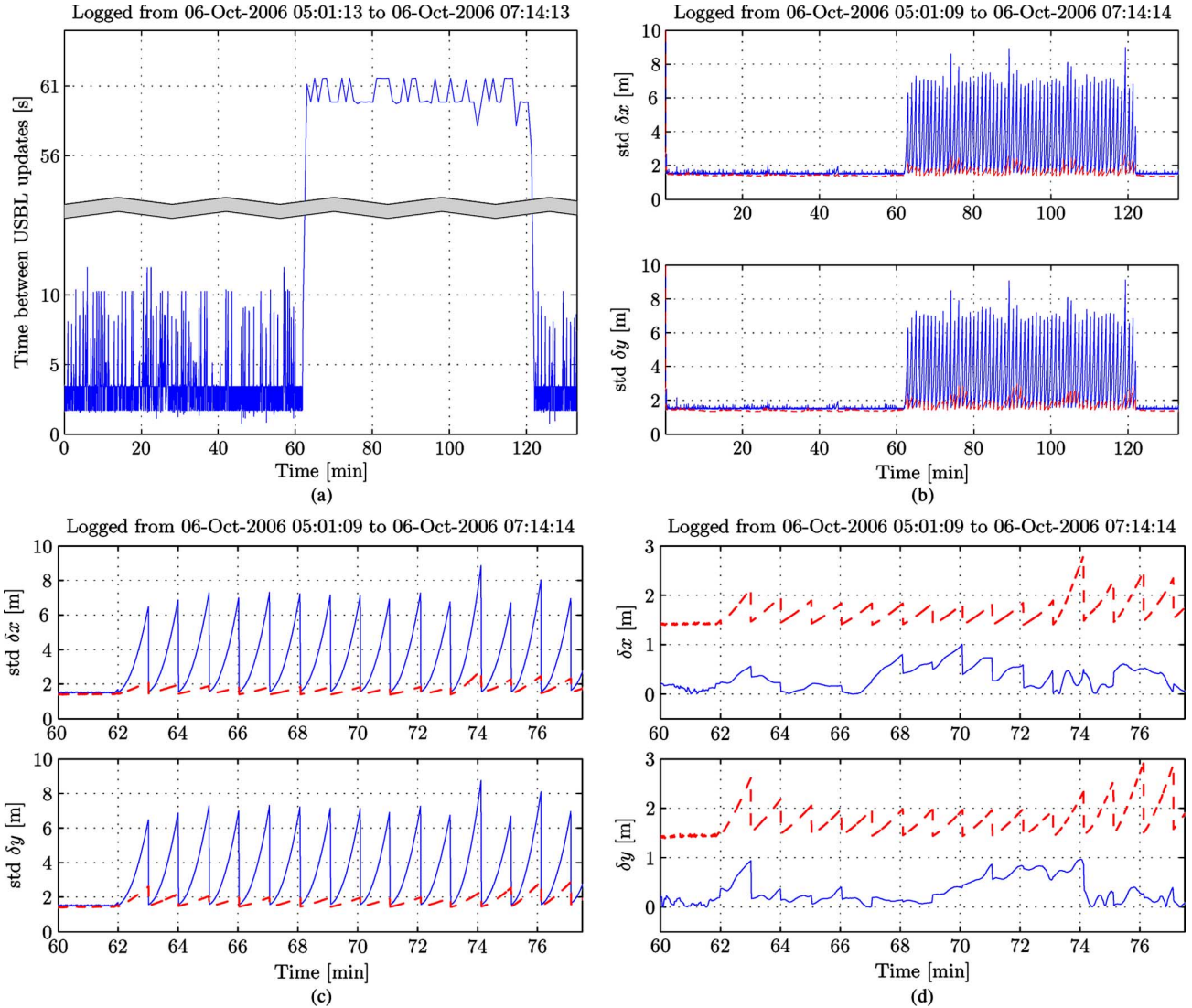


Fig. 18. Examples of USBL-INS and USBL-MA-INS performance with sparse or reduced frequency position updates: (a) The blue (solid) line shows the time between position measurements in Cases 1-2 and 2-2. (b) The KF real-time uncertainties in north and east (1σ) for the USBL-INS and the USBL-MA-INS are shown in blue (solid) and red (dashed), respectively. (c) Magnified version of Fig. 18(b). (d) The blue (solid) data show the absolute value of the north and east position errors for the USBL-MA-INS, according to Case 2-2. The corresponding KF real-time uncertainties (1σ) are shown in red (dashed).

to evaluate the performance of the integrated INS in cases where a DVL with bottom track is included in the navigation system sensor suite, but where measurements become unavailable. For instance, this will occur when (temporarily) operating above the sensor range or over rough bathymetry due to track loss. The first case is illustrated in Fig. 1. Other reasons may also be the cause of a DVL outage. Combined with few or no position measurement updates, the outcome may be damaging, and unacceptable for most autonomous or covert operations. Robustness, sustainability, and derisking are all key factors for mission success in these applications.

As earlier, the various conditions and results are summarized in Table V. With exception of temporary DVL outage, the conditions are identical to Cases 3-7, 3-8, 4-7, and 4-8 in Section IV-B3. The DVL outage scenario is best described from Fig. 15, where no bottom-track measurements are received while moving along the three line segments within the dashed area. Each of the lines corresponds to approximately 10 min.

As can be seen from the results summarized in Table V, the navigation performance of the USBL-DVL-MA-INS is superior to that obtained with the USBL-DVL-INS in both real time and when running RTS smoothing. While the latter navigation system is vulnerable to the DVL outage, the USBL-DVL-MA-INS is considerably more robust and is able to retain the sustainability and accuracy of the navigation system at a satisfactory level throughout. In fact, a closer look at Table V reveals that the performance of the USBL-DVL-MA-INS with DVL outage has worsened only slightly compared to the equivalent experiments in Section IV-B3, where DVL measurements are received regularly. This is particularly seen for the smoothed results. As for the performance of the conventional USBL-DVL-INS, it has deteriorated significantly in both real time and when doing RTS smoothing.

Additional plots comparing the USBL-DVL-INS and the USBL-DVL-MA-INS are shown in Fig. 20 for Cases 5-3 and 5-4. The maximum error of the real-time USBL-INS is about

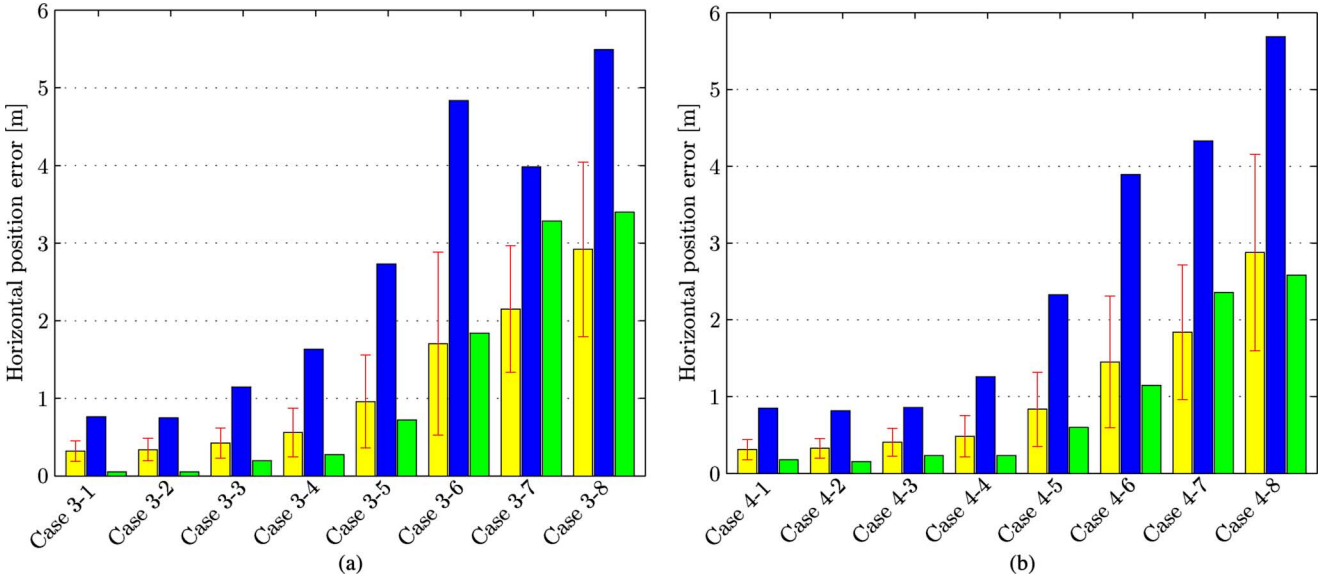


Fig. 19. Horizontal position estimation errors for Cases 3 and 4 in Table V. (a) The error bars from left to right show the mean and standard deviation of the real-time USBL-DVL-INS position error, the maximum real-time USBL-DVL-INS position error, and the maximum RTS smoothed USBL-DVL-INS position error. (b) Similar data and labels as in (a) but for the USBL-DVL-MA-INS. The performance of the latter navigation system is slightly better.

257 m. In the same scenario, and when including model aiding, the real-time horizontal position error is confined within 7.5 m. When doing RTS smoothing, the maximum position error in the latter system reduces to 3.5 m. The north and east INS position errors are for both navigation systems consistent with the KF covariances and within 1σ throughout. Similar results were also obtained for Cases 5-1 and 5-2. Together with the results obtained in Sections IV-B2 and IV-B3, this confirms the accuracy and robustness improvement of the MA-INS.

C. Remarks

While the results above clearly illustrate that the MA-INS is an effective and robust approach for limiting or reducing the position error drift it should be mentioned that other alternative aiding sources also exist. The analogous to using a kinetic vehicle model is to incorporate DVL water-track measurements in the navigation system [54]. The DVL water-track data are fairly accurate but the cost of the sensor may not be feasible to all. Opposed to model aiding, which is merely software, the DVL is also more vulnerable to environmental conditions, acoustic interference, and outage. Another promising velocity aid is micronavigation estimates [55] from a synthetic aperture sonar (SAS), also called displaced phase center antenna (DPCA). Potentially DPCA may provide an accuracy one order of magnitude better than high-quality DVL bottom track. Similar to the DVL, DPCA requires steady bottom track. It also imposes additional constraints on the vehicle stability. The cost of SAS is also high. Recall that while the use of velocity aiding alone restrains the INS velocity error growth, it cannot bound the position error drift indefinitely.

Another example is the application of terrain or feature-based positioning techniques [14], [56], [57]. These are able to bound the position error drift without the logistics associated with time-of-flight acoustics, hence making them suitable for autonomous and covert operations. Similar to DPCA and DVL bottom track, terrain-based techniques impose limitations on

the vehicle altitude. Special hardware is also required, though it is often part of the payload, e.g., multibeam echo sounders.

V. CONCLUSION

Despite significant efforts, precise navigation remains a substantial challenge to all underwater platforms. The actual autonomy of the vehicles in existence today is also limited. Further advances in both areas will enable new operations, which earlier have been considered impractical or infeasible. Enhanced accuracy and robustness, sustainability, and derisking are all key factors toward achieving these goals.

This paper reports the development and experimental evaluation of a complete MA-INS for underwater vehicle navigation. An accurate kinetic vehicle model has been derived, which provides external velocity aiding for the INS. In combination with embedded sea current estimation, the use of model aiding is shown to be an inexpensive and effective approach toward the solution of the aforementioned challenges, including improved navigation in the midwater zone, environmental estimation, and increased level of autonomy and robustness. A strong point of the approach is that it does not require any additional instrumentation. Also, since model aiding is merely an addition of software, the time between failure is extensive.

In addition to model aiding and sea current estimation, the navigation system integrates measurements from USBL and DVL with bottom track. The influence of including model aiding is investigated through several case scenarios, where DVL is or is not available and the position measurements are received at various rates. The effect of DVL outage is also explored. The experimental results verify that the MA-INS solution is superior to that obtained with the conventional INS when DVL measurements are unavailable. The difference in performance increases with decreasing USBL update rate. When also including DVL measurements the difference is smaller, yet in clear favor of the system with model aiding. During DVL outages, the MA-INS again performs significantly

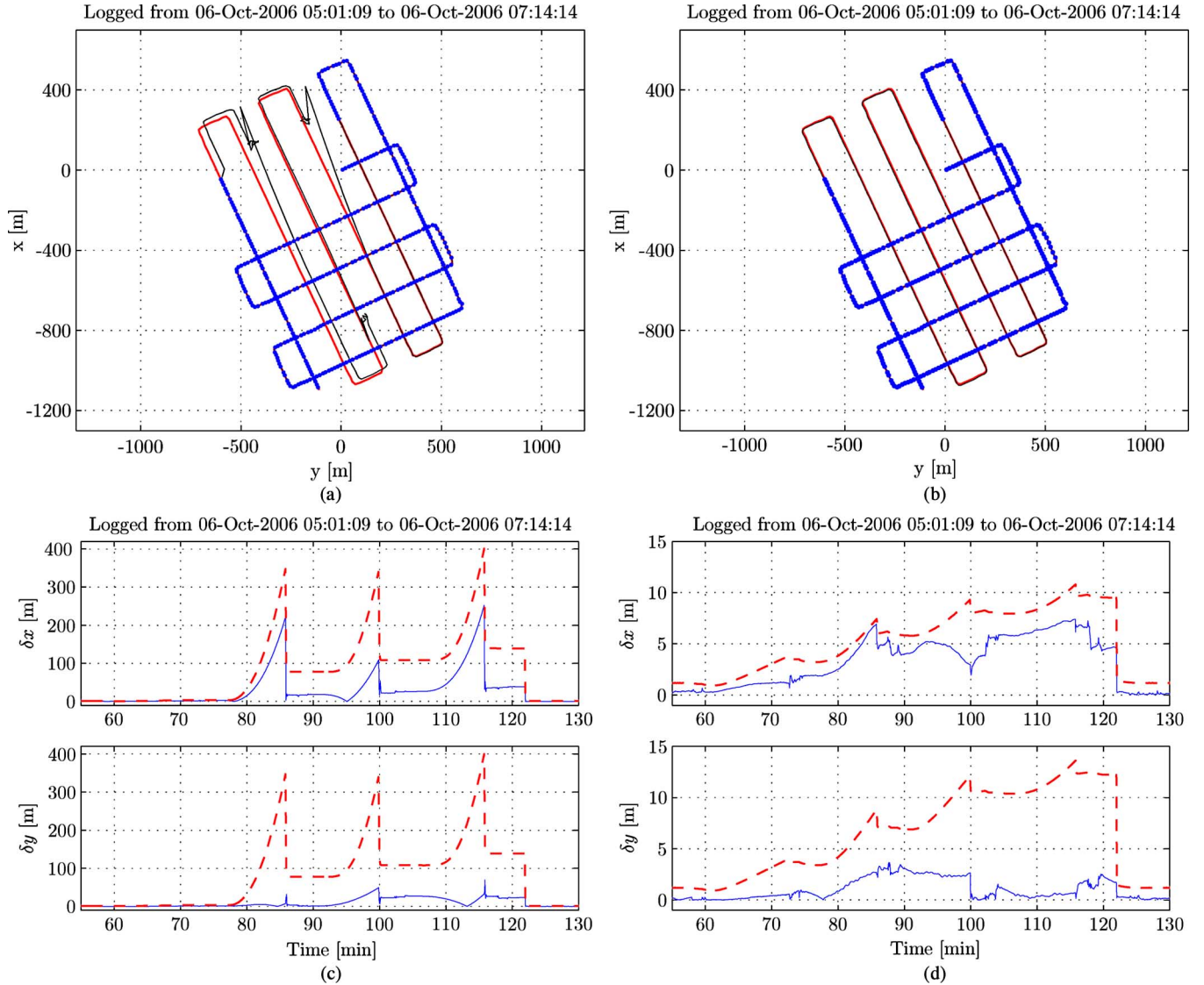


Fig. 20. Examples of USBL-DVL-INS and USBL-DVL-MA-INS performance with DVL outage and sparse position updates. (a) The red (solid) trajectory is the horizontal basis position, with its initial location at the origin. The blue “o” data show the position measurements. The total length of the segment with reduced position update frequency is 60 min, occurring between 62 and 122 min into the survey. In the considered examples no position measurements are received in this interval. At the same time, DVL measurements are lost when operating within the dashed area shown in Fig. 15. The real-time navigation solution obtained with the USBL-DVL-INS is shown in black (solid). (b) Similar labels and position measurements as in (a) but for USBL-DVL-MA-INS according to Case 5-4. The performance is significantly better than in the system without model aiding. (c) The blue (solid) data show the absolute value of the north and east position errors for the USBL-DVL-INS, according to Case 5-3. The corresponding KF real-time uncertainties (1σ) are shown in red (dashed). (d) Similar labels as in (c) but for USBL-DVL-MA-INS, according to Case 5-4.

better than the conventional system. For all the different scenarios it is found that the MA-INS is considerably more robust than the system not including model aiding, and it is able to keep the sustainability and accuracy of the navigation system at a satisfactory level even during long time periods without USBL and DVL measurements. As for the embedded sea current estimation it is found that the values show good agreement with an earlier reported LS solution. Besides being used for navigation, a current estimate may be of interest for other applications as well, such as oceanography and marine research, and autonomous mission planning and decision making.

ACKNOWLEDGMENT

Ø. Hegrenæs acknowledges the Kongsberg Maritime HUGIN engineers and the crew of *M/S Simrad Echo* for their help during

the experiments. The authors would like to thank B. Jalving and P. E. Hagen at Kongsberg Maritime, and E. Berglund and K. Gade at the Norwegian Defence Research Establishment for useful remarks and suggestions.

REFERENCES

- [1] J. C. Kinsey, R. M. Eustice, and L. L. Whitcomb, “A survey of underwater vehicle navigation: Recent advances and new challenges,” in *Proc. 7th IFAC Conf. Manoeuvring Control Marine Craft*, Lisbon, Portugal, Sep. 2006.
- [2] P. E. Hagen, T. G. Fossum, and R. E. Hansen, “Applications of AUVs with SAS,” in *Proc. MTS/IEEE OCEANS Conf. Exhibit*, Quebec, QC, Canada, Sep. 2008, DOI: 10.1109/OCEANS.2008.5152013.
- [3] P. E. Hagen, Ø. Hegrenæs, B. Jalving, Ø. Midtgård, M. Wiig, and O. K. Hagen, “Making AUVs truly autonomous,” in *Intelligent Underwater Vehicles*. Vienna, Austria: IN-TECH Education and Publishing, 2009, ch. 8.

- [4] M. Koifman and I. Bar-Itzhack, "Inertial navigation system aided by aircraft dynamics," *IEEE Trans. Control Syst. Technol.*, vol. 7, no. 4, pp. 487–493, Jul. 1999.
- [5] Ø. Hegrenæs, O. Hallingstad, and K. Gade, "Towards model-aided navigation of underwater vehicles," in *Proc. 15th Int. Symp. Unmanned Underwater Vehicles Technol.*, Durham, NH, Aug. 2007.
- [6] Ø. Hegrenæs, O. Hallingstad, and K. Gade, "Towards model-aided navigation of underwater vehicles," *Model. Identif. Control*, vol. 28, no. 4, pp. 113–123, Oct. 2007.
- [7] Ø. Hegrenæs, E. Berglund, and O. Hallingstad, "Model-aided inertial navigation for underwater vehicles," in *Proc. IEEE Int. Conf. Robot. Autom.*, Pasadena, CA, May 2008, pp. 1069–1076.
- [8] Y. Bar-Shalom, X. R. Li, and T. Kirubarajan, *Estimation With Applications to Tracking and Navigation*. New York: Wiley, 2001, ch. 2, 11, 12.
- [9] R. M. Eustice, L. L. Whitcomb, H. Singh, and M. Grund, "Experimental results in synchronous-clock one-way-travel-time acoustic navigation for autonomous underwater vehicles," in *Proc. IEEE Int. Conf. Robot. Autom.*, Rome, Italy, Apr. 2007, pp. 4257–4264.
- [10] B. Jalving, K. Gade, O. Hagen, and K. Vestgård, "A toolbox of aiding techniques for the HUGIN AUV integrated inertial navigation system," in *Proc. MTS/IEEE OCEANS Conf. Exhibit.*, San Diego, CA, Sep. 2003, vol. 2, pp. 1146–1153.
- [11] P. M. Lee, B. H. Jun, K. Kim, J. Lee, T. Aoki, and T. Hyakudome, "Simulation of an inertial acoustic navigation system with range aiding for an autonomous underwater vehicle," *IEEE J. Ocean. Eng.*, vol. 32, no. 2, pp. 327–345, Apr. 2007.
- [12] A. Alcocer, P. Oliveira, and A. Pascoal, "Study and implementation of an EKF GIB-based underwater positioning system," *Control Eng. Practice*, vol. 15, no. 6, pp. 689–701, Jun. 2007.
- [13] K. B. Ånonsen and O. Hallingstad, "Terrain aided underwater navigation using point mass and particle filters," in *Proc. IEEE/ION Position Location Navigat. Symp.*, San Diego, CA, Apr. 2006, pp. 1027–1035.
- [14] K. B. Ånonsen and O. Hallingstad, "Sigma point Kalman filter for underwater terrain-based navigation," in *Proc. IFAC Conf. Control Appl. Marine Syst.*, Bol, Croatia, Sep. 2007, DOI: 10.3182/20070919-3-HR-3904.00020.
- [15] A. B. Willumsen, O. Hallingstad, and B. Jalving, "Integration of range, bearing and Doppler measurements from transponders into underwater vehicle navigation systems," in *Proc. MTS/IEEE OCEANS Conf. Exhibit.*, Boston, MA, Sep. 2006, DOI: 10.1109/OCEANS.2006.306851.
- [16] A. Gadre and D. Stilwell, "A complete solution to underwater navigation in the presence of unknown currents based on range measurements from a single location," in *Proc. IEEE/RSJ Int. Conf. Intell. Robots Syst.*, Edmonton, ON, Canada, Aug. 2005, pp. 1420–1425.
- [17] J. Jouffroy and J. Opderbecke, "Underwater vehicle navigation using diffusion-based trajectory observers," *IEEE J. Ocean. Eng.*, vol. 32, no. 2, pp. 313–326, Apr. 2007.
- [18] J. C. Kinsey and L. L. Whitcomb, "Model-based nonlinear observers for underwater vehicle navigation: Theory and preliminary experiments," in *Proc. IEEE Int. Conf. Robot. Autom.*, Rome, Italy, Apr. 2007, pp. 4251–4256.
- [19] J. E. Refsnæs, A. J. Sørensen, and K. Y. Pettersen, "A 6 DOF nonlinear observer for AUVs with experimental results," in *Proc. 15th IEEE Mediterranean Conf. Control Autom.*, Athens, Greece, Jun. 2007, DOI: 10.1109/MED.2007.4433891.
- [20] J. E. Refsnæs and A. J. Sørensen, "Comparison of two linear observers for marine vessels," in *Proc. IFAC Conf. Control Appl. Marine Syst.*, Bol, Croatia, Sep. 2007, DOI: 10.3182/20070919-3-HR-3904.00007.
- [21] T. Pfuetzenreuter, T. Rauschenbach, and J. Wernstedt, "Multisensor fusion for navigation of underwater vehicles," in *Proc. IEEE Int. Conf. Multisensor Fusion Integr. Intell. Syst.*, Heidelberg, Germany, Sep. 2006, pp. 151–154.
- [22] M. Bryson and S. Sukkarieh, "Vehicle model aided inertial navigation for a UAV using low-cost sensors," in *Proc. Australasian Conf. Robot. Autom.*, Canberra, Australia, Dec. 2004.
- [23] J. F. Vasconcelos, C. Silvestre, and P. Oliveira, "Embedded vehicle dynamics and laser aiding techniques for inertial navigation systems," in *Proc. AIAA Guid. Navigat. Control Conf.*, Keystone, CO, Aug. 2006, Article: AIAA2006-6581.
- [24] M. Morgado, P. Oliveira, C. Silvestre, and J. Vasconcelos, "Vehicle dynamics aiding technique for USBL/INS underwater navigation system," in *Proc. IFAC Conf. Control Appl. Marine Syst.*, Bol, Croatia, Sep. 2007, DOI: 10.3182/20070919-3-HR-3904.00021.
- [25] T. Nicosevic, R. Garcia, M. Carreras, and M. Villanueva, "A review of sensor fusion techniques for underwater vehicle navigation," in *Proc. MTS/IEEE OCEANS Conf. Exhibit.*, Kobe, Japan, Nov. 2004, vol. 3, pp. 1600–1605.
- [26] Ø. Hegrenæs, O. Hallingstad, and B. Jalving, "A comparison of mathematical models for the HUGIN 4500 AUV based on experimental data," in *Proc. IEEE Int. Symp. Underwater Technol.*, Tokyo, Japan, Apr. 2007, pp. 558–567.
- [27] M. Gertler and S. C. Hagen, "Standard equations of motion for submarine simulations," Naval Ship Res. Develop. Ctr., Washington, DC, Tech. Rep. DTMB 2501, 1967.
- [28] J. Feldman, "DTMSRDC revised standard submarine equations of motion," Naval Ship Res. Develop. Ctr., Washington, DC, Tech. Rep. DTNSRDC-SPD-0393-09, 1979.
- [29] T. Prestero, "Verification of a six-degree of freedom simulation model for the REMUS autonomous underwater vehicle," M.S. thesis, Dept. Ocean Eng., Massachusetts Inst. Technol., Cambridge, MA, 2001.
- [30] P. Ridley, J. Fontan, and P. Corke, "Submarine dynamic modeling," in *Proc. Australasian Conf. Robot. Autom.*, Brisbane, Australia, Dec. 2003.
- [31] M. Caccia, G. Indiveri, and G. Veruggio, "Modeling and identification of open-frame variable configuration unmanned underwater vehicles," *IEEE J. Ocean. Eng.*, vol. 25, no. 2, pp. 227–240, Apr. 2000.
- [32] D. A. Smallwood, "Advances in dynamical modeling and control of underwater robotic vehicles," Ph.D. dissertation, Dept. Mech. Eng., Johns Hopkins Univ., Baltimore, MD, 2003.
- [33] M. Nahon, "Determination of undersea vehicle hydrodynamic derivatives using the USAF DATCOM," in *Proc. IEEE Oceans Conf. Exhibit.*, Victoria, BC, Canada, Oct. 1993, vol. 2, pp. 283–288.
- [34] Ø. Hegrenæs, O. Hallingstad, and B. Jalving, "A framework for obtaining steady-state maneuvering characteristics of underwater vehicles using sea-trial data," in *Proc. 15th IEEE Mediterranean Conf. Control Autom.*, Athens, Greece, Jun. 2007, DOI: 10.1109/MED.2007.4433900.
- [35] K. Gade, "A non-singular horizontal position representation," *J. Navig.*, vol. 63, no. 3, pp. 395–417, Jul. 2010, DOI: 10.1017/S037346330990415.
- [36] SNAME Technical and Research Committee, "Nomenclature for treating the motion of a submerged body through a fluid," Soc. Naval Architects Marine Eng. (SNAME), New York, Tech. Rep. Tech. Res. Bull. No. 1–5, 1950.
- [37] O. Egeland and J. T. Gravdahl, *Modeling and Simulation for Automatic Control*. Trondheim, Norway: Marine Cybernetics, 2002, ch. 6, 14.
- [38] T. I. Fossen, *Marine Control Systems: Guidance, Navigation and Control of Ships, Rigs and Underwater Vehicles*. Trondheim, Norway: Marine Cybernetics, 2002, ch. 3.
- [39] D. E. Humphreys and K. W. Watkinson, "Prediction of acceleration hydrodynamic coefficients for underwater vehicles from geometric parameters," Naval Coastal Syst. Lab., Panama City, FL, Tech. Rep. NCSL-TR-327-78, Feb. 1978.
- [40] F. S. Malvestuto and L. J. Gale, "Formulas for additional mass corrections to the moments of inertia of airplanes," Nat. Advisory Committee Aeronaut., Tech. Rep. NACA No. 1187, 1947.
- [41] R. D. Blevins, *Formulas for Natural Frequency and Mode Shape*. Malabar, FL: R.E. Krieger, 1984, ch. 14.
- [42] R. D. Finck and D. E. Hoak, *USAF Stability and Control DATCOM*. Wright-Patterson AFB, Ohio: Wright-Patterson Airforce Base, Apr. 1978.
- [43] S. F. Hoerner and H. V. Borst, *Fluid-Dynamic Lift: Practical Information on Aerodynamic and Hydrodynamic Lift*. Brick Town, NJ: Hoerner Fluid Dynamics, 1975.
- [44] S. F. Hoerner, *Fluid-Dynamic Drag: Practical Information on Aerodynamic Drag and Hydrodynamic Resistance*. Brick Town, NJ: Hoerner Fluid Dynamics, 1965.
- [45] B. W. McCormick, *Aerodynamics, Aeronautics, and Flight Mechanics*, 2nd ed. New York: Wiley, 1994, ch. 3, 4.
- [46] Ø. Hegrenæs, "Open-water propulsion test using full-scale propellers for the HUGIN AUV family," Univ. Grad. Ctr., Kjeller, Norway, Tech. Rep., 2006.
- [47] K. Gade, "NavLab, a generic simulation and post-processing tool for navigation," *Eur. J. Navigat.*, vol. 2, no. 4, pp. 21–59, Nov. 2004.
- [48] B. Jalving, K. Gade, K. Svartveit, A. Willumsen, and R. Sørhagen, "DVL velocity aiding in the HUGIN 1000 integrated inertial navigation system," *Model. Identif. Control*, vol. 25, no. 4, pp. 223–235, 2004.
- [49] K. Gade, "Integrering av treghetsnavigasjon i en autonom undervannsfarkost," (in Norwegian) Norwegian Defence Res. Establishment (FFI), Kjeller, Norway, Tech. Rep. FFI/RAPPORT-97/03179, 1997.
- [50] A. Gelb, *Applied Optimal Estimation*. Cambridge, MA: MIT Press, 1974, ch. 2.
- [51] X. R. Li and V. P. Jilkov, "Survey of maneuvering target tracking—Part I: Dynamic models," *IEEE Trans. Aerosp. Electron. Syst.*, vol. 39, no. 4, pp. 1333–1364, Oct. 2003.

- [52] B. Jalving, K. Vestgård, and N. Størkersen, "Detailed seabed surveys with AUVs," in *Technology and Applications of Autonomous Underwater Vehicles*, G. Griffiths, Ed. London, U.K.: Taylor & Francis, 2003, vol. 2, pp. 179–201.
- [53] Ø. Hegrenæs, K. Gade, O. K. Hagen, and P. E. Hagen, "Underwater transponder positioning and navigation of autonomous underwater vehicles," in *Proc. IEEE OCEANS Conf. Exhibit.*, Biloxi, MS, Oct. 2009.
- [54] Ø. Hegrenæs and E. Berglund, "Doppler water-track aided inertial navigation for autonomous underwater vehicles," in *Proc. IEEE OCEANS Conf. Exhibit.*, Bremen, Germany, May 2009, DOI: 10.1109/OCEANSE.2009.5278307.
- [55] R. E. Hansen, T. O. Sæbø, K. Gade, and S. Chapman, "Signal processing for AUV based interferometric synthetic aperture sonar," in *Proc. MTS/IEEE OCEANS Conf. Exhibit.*, San Diego, CA, Sep. 2003, vol. 5, pp. 2438–2444.
- [56] O. K. Hagen, "TerrLab—A generic simulation and post-processing tool for terrain referenced navigation," in *Proc. MTS/IEEE OCEANS Conf. Exhibit.*, Boston, MA, Sep. 2006, DOI: 10.1109/OCEANS.2006.306834.
- [57] R. M. Eustice, "Large-area visually augmented navigation for autonomous underwater vehicles," Ph.D. dissertation, Dept. Ocean Eng., Massachusetts Inst. Technol., Cambridge, MA, 2005.



Øyvind Hegrenæs (S'06–M'08) was born in Bergen, Norway, in 1979. He received the M.S. and Ph.D. degrees in engineering cybernetics from the Norwegian University of Science and Technology (NTNU), Trondheim, Norway, in 2004 and 2010, respectively. Part of his studies was carried out at the Department of Mechanical Engineering, University of California Berkeley, Berkeley, in 2002–2003, and at the Dynamical Systems and Control Laboratory, Johns Hopkins University, Baltimore, MD, in 2005. His Ph.D. research focused on inertial navigation of autonomous underwater vehicles (AUVs), and the use of alternative aiding techniques for enabling new application of AUVs by improving the accuracy, robustness, and sustainability of the integrated navigation system.

Since 2008, he has been part of the HUGIN AUV team at Kongsberg Maritime, Horten, Norway, where he is responsible for navigation.

Dr. Hegrenæs received the National IFAC Member Organization prize for best M.S. thesis within automatic control in Norway in 2004.



Oddvar Hallingstad (M'90) was born in Hol, Norway, in 1945. He received the M.E. and Ph.D. degrees in engineering cybernetics from the Norwegian Technical University (NTH), Trondheim, Norway, in 1971 and 1978, respectively.

He joined the Norwegian Defence Research Establishment (FFI), Kjeller, Norway, in 1977, where he worked on the inertial navigation system for the new coastal vessels and the inertial navigation system for the Penguin air to sea missile. Since 1989, he has been at the Graduate University Center at Kjeller (UniK), Kjeller, Norway, lecturing estimation theory and being an advisor for Master and Ph.D. students. He is also an Adjunct Professor at the Norwegian University of Science and Technology (NTNU) and a part-time employee at FFI.

Kjeller, Norway, lecturing estimation theory and being an advisor for Master and Ph.D. students. He is also an Adjunct Professor at the Norwegian University of Science and Technology (NTNU) and a part-time employee at FFI.